ELSEVIER

Physica D 144 (2000) 387–433

PHYSICA D

www.elsevier.com/locate/physd

Real topological entropy versus metric entropy for birational measure-preserving transformations

N. Abarenkova [a,b], J.-Ch. Anglès d'Auriac [a,*], S. Boukraa [c,d], J.-M. Maillard [c]

[a] *Centre de Recherches sur les Très Basses Températures, BP 166, F-38042 Grenoble, France*
[b] *Theoretical Physics Department, St. Petersburg State University, Ulyanovskaya 1, 198904 St. Petersburg, Russia*
[c] *LPTHE, Tour 16, 1er étage, 4 Place Jussieu, 75252 Paris Cedex, France*
[d] *Institut d'Aéronautique, Université de Blida, BP 270, Blida, Algeria*

Received 7 July 1999; received in revised form 5 January 2000; accepted 1 March 2000
Communicated by J.D. Meiss

Abstract

We consider a family of birational measure-preserving transformations of two complex variables, depending on one parameter for which simple rational expressions for the dynamical zeta function have been conjectured, together with an equality between the topological entropy and the logarithm of the Arnold complexity (divided by the number of iterations). Similar results have been obtained for the adaptation of these two concepts to dynamical systems of real variables, yielding to introduce a "real topological entropy" and a "real Arnold complexity". We try to compare, here, the Kolmogorov–Sinai metric entropy and this real Arnold complexity, or real topological entropy, on this particular example of a one-parameter dependent birational transformation of two variables. More precisely, we analyze, using an infinite precision calculation, the Lyapunov characteristic exponents for various values of the parameter of the birational transformation, in order to compare these results with the ones for the real Arnold complexity. We find a quite surprising result: for this very birational example, and, in fact, for a large set of birational measure-preserving mappings generated by involutions, the Lyapunov characteristic exponents seem to be equal to zero or, at least, extremely small, for all the orbits we have considered, and for all values of the parameter. Birational measure-preserving transformations, generated by involutions, could thus allow to better understand the difference between the topological description and the probabilistic description of discrete dynamical systems. Many birational measure-preserving transformations, generated by involutions, seem to provide examples of discrete dynamical systems which can be topologically chaotic while they are metrically almost quasi-periodic. Heuristically, this can be understood as a consequence of the fact that their orbits seem to form some kind of "transcendental foliation" of the two-dimensional space of variables.

PACS: 05.45.+b; 03.20; 46.10; 47.52.+j; 05.50.+q; 02.90.+p

Keywords: Kolmogorov–Sinai metric entropy; Lyapunov characteristic exponents; Arnold complexity; Topological entropy; Discrete dynamical systems of real variables; Measure-preserving maps; Birational mappings; Cremona transformations; Rational dynamical zeta functions; Complex mappings versus real mappings; Transcendental foliations

* Corresponding author.
E-mail addresses: dauriac@polycnrs-gre.fr (J.-Ch. Anglès d'Auriac), maillard@lpthe.jussieu.fr (J.-M. Maillard).

0167-2789/00/$ – see front matter
PII: S0167-2789(00)00079-8

1. Introduction

To study the complexity of continuous or discrete dynamical systems, a large number of concepts have been introduced [1,2]. A non-exhaustive list includes the Kolmogorov–Sinai metric entropy [3,4], the Adler–Konheim–McAndrew topological entropy [5], the Arnold complexity [6], the Lyapunov characteristic exponents, the various fractal dimensions [7,8], the Feigenbaum's numbers of period doubling cascades [9,10], etc. Many authors have tried to study and discuss the relations between these various notions in an abstract framework [11,12]. Inequalities have been shown: for instance the Kolmogorov–Sinai metric entropy is bounded by the topological entropy, and one can also mention the Kaplan–Yorke relation [13,14]. Furthermore, many specific dynamical systems have been introduced enabling to see these notions at work. Some of the most popular are the Lorentz system [15], the baker map [16], the logistic map [17], the Hénon map [18]. Each of these systems has been useful to understand and exemplify the previous complexity notions.

As far as dynamical systems are concerned one must say that there exist a quite sharp cultural difference between physicists and mathematicians. In its most extreme form, physicists will consider as (physically) interesting the mappings of a unique [1] variable for which some results can be obtained, or, at least, some calculations can be performed, like the mappings of the interval, the zig-zag maps, the logistic map, and two "historical" systems of more than one variable, the Hénon map and the Lorentz system, and mathematicians will consider as (mathematically) interesting the continuous (differentiable) systems (flows) for which theorems can be obtained, namely hyperbolic systems which can be seen as smooth diffeomorphisms on smooth compact spaces.

However, if one does not have such prejudice, and is only willing to study the dynamical systems that occur in true nonlinear physical phenomena, one is led to study dynamical systems of several variables which are neither hyperbolic [19] nor smooth, and present some mix between regularity and chaos. Very few results are available. In particular one would like to build some new tools in order to describe and understand the "complexity" of such multi-dimensional dynamical systems. We want to understand, beyond the well-known phenomena occurring with very few variables and widely described in the literature on chaos (strange attractors, period doubling, etc.), what physics comes specifically from the occurrence of several variables (Arnold diffusion, etc.).

In this respect, polynomial transformations of several variables are the most natural and simple mappings to study. In fact, the computer analysis of dynamical systems very often amounts to performing (quite uncontrolled) sneaking polynomial truncations of the "true" systems. To be numerically rigorous one should compare a large set of polynomial truncations and take into account only the results that are unchanged according to these various truncations. This yields a strong (numerical) bias in favor of polynomials, and even polynomial iterations on rational numbers. It should be noticed that the physics of polynomial mappings of several variables tends (generically) to be dominated by the collapse to a few attracting fixed points, and by some features already encountered with mappings of very few variables and corresponding to the (generically) irreversible character of the polynomial mappings (strange attractors, period doubling, etc.). Therefore the next step, in order to get some interesting, or simply new, physics, amounts to considering polynomial or rational transformations (so that many computer numerical or formal calculations can actually be performed), which are reversible, in order to get some interesting new features for the phase space. This allows to consider birational transformations [23,24]. This set of transformations is particularly interesting from a numerical point of view, since one can totally control the calculations (see below). Actually let us recall that birational transformations naturally occur in lattice statistical mechanics, in the framework of Yang–Baxter equations, and, beyond, occur canonically as (infinite discrete) symmetries of the phase diagrams of the lattice models

[1] In this respect renormalization type arguments are used to argue that the true multi-dimensional systems (turbulence, etc.) will reduce, at the end of the day, to dynamical systems of very few variables. In addition, one can also argue that dynamical systems with very few variables actually exhibit some features of the true multi-dimensional systems (see, for instance [20–22]).

[25,26] far beyond the very narrow framework Yang–Baxter integrable models. Unfortunately, the set of birational transformations is, generically, a huge one and, furthermore, the problem of the proliferation of singularities, in the iteration process, is a very serious and involved one. However, let us emphasize that the birational transformations inherited from lattice statistical mechanics are, in fact, birational transformations generated by involutions that happen to be measure-preserving maps. Therefore, we are not considering the most general (and mathematically difficult) framework of the most general birational transformations, but a more "controlled" framework of birational measure-preserving transformations generated by involutions, thus providing naturally some nice reversibility and regularity for the dynamical system. Let us, however, underline that a reversible measure-preserving transformation can yield an extremely involved non-trivial dynamical system: its Kolmogorov–Sinai metric entropy, or its Lyapunov characteristic exponents, have no reason to be equal to zero, neither its topological entropy.

We want to study such dynamical systems of many variables in this physically interesting framework (weak chaos, nearly conservative systems). Our study is mostly a (infinite precision) numerical study, together with formal calculations and exact analytical calculations (Section 6.1) and amounts to filing the gap between two approaches of complexity of dynamical systems: the topological approach and "measure" (probabilistic) approach of dynamical systems.

We would like to recall that birational transformations have not been extensively studied by mathematicians because, from a mathematical point of view, one can expect, at first sight, some unpleasant, and uncontrolled, proliferation of singularities. There is, however, some mathematical literature on this subject: among the few papers concerning birational transformations one can cite Diller [27,28], as well as Favre [29], and also Russakovskii and Shiffman [30]. Most of these papers heavily rely on complex analysis and are mainly concerned by the so-called "general" or "typical" mappings, namely mappings such that the degree of the Nth iterate of a mapping of degree d is d^N. The problem with these general or typical mappings is that the various entropies one can introduce tend to identify with the logarithm of this degree d: therefore, these typical mappings are not very well suited to classify, compare and discriminate these various entropies. It should be noticed that the family of mappings we will study here are not of this general–typical type: the degree of their Nth iterate grows like λ^N, where $\lambda < d$. This family is thus well suited to be analyzed according to various entropy points of view (Arnold complexity, topological entropy, Kolmogorov–Sinai metric entropy, etc.).

In order to study the rich and non-trivial physics of the birational measure-preserving transformations generated by involutions, we will thus consider a family of birational transformations of two complex variables, depending on one parameter: this one-parameter family [2] of maps is a particularly interesting test family as it is integrable for a certain set of values of the parameter, has non-generic behavior at a certain countable set of values of the parameter, and has generic behavior at all other values [31,32]. Considering this specific family of birational transformations of two complex variables, depending on one parameter, simple exact rational expressions with integer coefficients, have been conjectured for their dynamical zeta function [33], together with an equality between the (multiplicative rate of growth of the) Arnold complexity and the (exponential of the) topological entropy [34,35]. These two complexities have been shown to be associated with algebraic values for many birational mappings, possibly, all the birational mappings, and possibly also, all the rational mappings [36]. However, the previous equality is probably not valid for any rational, or even birational, transformation (see Section 2.4). On this very example, it has been found that the identification of these two universal (or topological) evaluations of the complexities [33,34], namely the logarithm of the Arnold complexity [6] (divided by the number of iterations) and the topological entropy [34], also applies to the "adaptation" of these two notions to real analysis introduced in a previous paper [37], i.e. if one restricts the mapping to two real variables.

[2] This mapping originates from an exhaustive analysis of mappings generated by the composition of matrix inversion and permutation of entries of 3×3 matrices [31].

The purpose of this paper is to compare the Kolmogorov–Sinai metric entropy [38,39] and this adaptation of the topological entropy [34] (or of the Arnold complexity) to real analysis. More precisely, we will compare the metric entropy, or, practically, as many Lyapunov exponents as possible, and this real topological entropy on a particular example of a one-parameter dependent birational transformation of two variables. In other words, we want to compare the real topological description of discrete dynamical systems with the metric description, on a specific two-dimensional birational example. This test family will explain how a mapping can look metrically almost-periodic and be topologically chaotic at the same time, even as far as real analysis is concerned.

Let us give a brief outline of the paper. We will first recall, in Section 2, some previous results [3] and notations, concerning the topological entropy and the Arnold complexity, as well as their adaptations to real analysis. We will then compare these topological notions with the metric entropy, or more precisely the characteristic Lyapunov exponents. For this purpose we will display a large set of phase portraits and Lyapunov characteristic exponents. We will provide a heuristic interpretation of the results, as well as a detailed study of a particular case, $\epsilon = 3$. In order to better understand the role played by the reversibility and measure-preserving properties in these results we will consider two deformations of the mapping: a birational deformation breaking the measure-preserving property and a rational deformation breaking the reversibility property. The conclusion will summarize the mechanisms occurring in the topological-chaos versus metric-almost-integrability situation described here.

2. Topological entropy and growth (Arnold) complexity for a one-parameter family of birational mapping

2.1. A measure-preserving mapping generated by two involutions

Let us consider the following birational transformation k_ϵ (see (3) in [33]) of two (complex) variables depending on one parameter ϵ:

$$k_\epsilon : (y, z) \to \left(z + 1 - \epsilon, y\frac{z-\epsilon}{z+1}\right). \tag{1}$$

This birational transformation can be seen to be the product of two involutions [23,24,31]. This map is the product of two involutions $I_1 : (y, z) \leftrightarrow (-z, -y)$ and

$$I_2 : (y, z) \to (y', z') = \left(-\frac{z-\epsilon}{z+1}y, \epsilon - 1 - z\right). \tag{2}$$

These two involutions I_1 and I_2 have the lines $z = -y$ and $z = \frac{1}{2}(\epsilon - 1)$ as fixed point sets, respectively. The inverse transformation k_ϵ^{-1} is nothing but transformation (1) where $y \leftrightarrow -z$:

$$(y, z) \to (y', z') = \left(\frac{y+\epsilon}{y-1}z, \epsilon - 1 + y\right). \tag{3}$$

There exists, for this mapping, a singled-out globally invariant line $y = 1 + z$, on which the mapping just reduces to a simple translation: $y \to y - \epsilon$.

Mapping (1) has a remarkable property: it is a measure-preserving mapping [40]. A measure-preserving mapping is a mapping that is conjugate to an area-preserving mapping: it can be rewritten, up to a quite complicated, and possibly singular transformation, into an area-preserving map [40]. Measure-preserving mappings were studied by Poincaré [41].

[3] Note, however, that Sections 2.1 and 2.4 provide new results.

Calculating the Jacobian of transformation (1), one gets

$$\det\begin{bmatrix} \dfrac{dy'}{dy} & \dfrac{dz'}{dy} \\ \dfrac{dy'}{dz} & \dfrac{dz'}{dz} \end{bmatrix} = \det\begin{bmatrix} 0 & \dfrac{z-\epsilon}{z+1} \\ 1 & \dfrac{y(1+\epsilon)}{(z+1)^2} \end{bmatrix} = -\frac{z-\epsilon}{z+1}. \tag{4}$$

Let us note that the line $y = z + 1$ is a line where the successive points of the iterations seem to accumulate (see [37]). As far as seeking for an invariant measure for mapping (1) is concerned, one should thus have a higher density of iterated points near this singled-out line. The line $y = z + 1$ is actually a globally invariant line on which transformation (1) reduces to a simple translation as

$$k_\epsilon : (y, z) \to (y - \epsilon, z - \epsilon). \tag{5}$$

Clearly, no fixed points of any order can exist on this singled-out line. For generic values of ϵ, this corresponds to the only (algebraic) covariant of transformation (1), namely $c(y, z) = y - 1 - z$ (of course, they are many more, say for integrable values of ϵ, etc.). Under transformation (1), the covariant $c(y, z) = y - 1 - z$ transforms with a cofactor which is nothing but the Jacobian (4):

$$k_\epsilon : y - 1 - z \to y' - 1 - z' = -\frac{z-\epsilon}{z+1}(y - 1 - z). \tag{6}$$

In other words, the Jacobian can always be written as the ratio $c(y', z')/c(y, z)$ (where $c(y', z')$ is the covariant taken at the image point (y', z')). This is the key ingredient for having a measure-preserving map (see relation (2.20) in [40]). Actually, introducing a change of variables $(y, z) \to (u, v)$ such that the Jacobian of this change of variables will be equal to the inverse of this covariant, one will change our measure-preserving map into an area-preserving map:

$$\det\begin{bmatrix} \dfrac{du}{dy} & \dfrac{dv}{dy} \\ \dfrac{du}{dz} & \dfrac{dv}{dz} \end{bmatrix} = \frac{1}{y-1-z}. \tag{7}$$

There are an infinite number of such change of variables. One (not very elegant) solution amounts to imposing $(u, v) = (y, v(y, z))$, the Jacobian (7) reading:

$$\frac{dv}{dy} = \frac{1}{y-1-z}, \tag{8}$$

which can be easily integrated into $v = \ln(y - 1 - z)$, its inverse being $(y, z) = (u, u - e^v - 1)$. Rewriting the mapping in these (u, v) variables one gets

$$(u, v) \to (u', v') = (u - e^v - \epsilon, v + \ln(V)), \quad V = \frac{u - e^v - 1 - \epsilon}{e^v - u}. \tag{9}$$

One easily verifies that mapping (9) has a Jacobian equal to 1 everywhere. It is an area-preserving map.

As far as the forthcoming topological notions are concerned (dynamical zeta functions, Arnold complexity, topological entropy, etc.), it is clear that they remain unchanged for the area-preserving mapping (9).

One can easily deduce the following consequence from the measure-preserving property of the mapping: the Jacobian of k^N is equal to 1 at every fixed point of k^N for any N. Of course the Jacobian is not equal to 1 everywhere, except for an area-preserving map.

Remark 1. *In* [32], *it has been shown that, in spite of its simplicity, birational mapping* (1) *can, however, have quite different behaviors according to the actual values of the parameter* ϵ. *For example, for* $\epsilon = 0$, *as well as* $\epsilon = -1,\ \frac{1}{2},\ \frac{1}{3}$ or 1, *the mapping becomes* integrable [32], *whereas it is not integrable for all other values of* ϵ. *Other singled-out values of* ϵ *occur* [33–35], *namely* $\epsilon = 1/m$, *where* $m \geq 4$ *and* $\epsilon = (m-1)/(m+3)$ *where m is odd and* $m \geq 7$. *For these singled-out values of* ϵ, *the topological entropy gets smaller as compared to a generic value* [33–35] (*see* (15)).

Remark 2. *From a mathematical point of view birational transformations might look difficult to analyze because one can expect, at first sight, some unpleasant proliferation of singularities. Let us just point here that, fortunately, we are in a very favorable situation and the* indeterminacy locus [4] *is far from being a dense set: it is very tame for mappings* (1). *From Jacobian* (4), *one gets that the critical locus is the line* $z = \epsilon$, *its critical image being the point* $(y, z) = (1, 0)$. *This is a point of indeterminacy for* k_ϵ^{-1}. *By inspection* (*or from the* $y \leftrightarrow -z$ *symmetry*) *the point of indeterminacy for* k_ϵ *is* $(y, z) = (0, -1)$. *Both critical points belong to the singled-out line* $y = 1 + z$ *on which the action of* k_ϵ (*or* k_ϵ^{-1}) *reduces to a simple shift* (*see* 5). *The backward and forward iterates of these two critical points can thus be easily described.* [5] *The point of indetermination at infinity for* k_ϵ *is* $(y, z) = (\infty, 0)$ (*resp.* $(y, z) = (0, \infty)$ *for* k_ϵ^{-1}).

2.2. Topological entropy

It is well known that the periodic orbits (cycles) of a mapping k strongly characterize dynamical systems [43]. The fixed points of the Nth power of the mapping being the cycles of the mapping itself, their proliferation with N provides an evaluation of chaos [2]. [6] To keep track of this number of cycles, one can introduce the fixed points generating function

$$H(t) = \sum_{N=1}^{\infty} \#\mathrm{fix}(k^N) t^N, \tag{10}$$

where $\#\mathrm{fix}(k^N)$ is the number of fixed points of k^N, real or complex. This quantity only depends on the number of fixed points, and not on their particular localizations. In this respect, $H(t)$ is a topologically invariant quantity. In an equivalent way, the same information can also be encoded in the so-called [7] dynamical zeta function $\zeta(t)$ [45,46] related to the generating function $H(t)$ by $H(t) = t(\mathrm{d}/\mathrm{d}t)\log(\zeta(t))$. The dynamical zeta function is defined as follows [43,44,46–49]:

$$\zeta(t) = \exp\left(\sum_{N=1}^{\infty} \#\mathrm{fix}(k^N) \frac{t^N}{N}\right). \tag{11}$$

The topological entropy [5,44–46], $\log h$, is therefore defined [8] by

[4] In this respect one should mention the paper by Nishimura [42], where birational maps are classified in terms of their points of indeterminacy.

[5] Furthermore, this also enables to understand why the singled-out values $\epsilon = 1/m,\ m = 1, 2, 3, 4, \ldots$ are special.

[6] Chaos: Classical and Quantum — a web book to be found on Cvitanovic's web site http://www.nbi.dk/ChaosBook.

[7] The dynamical zeta function has been introduced by analogy with the Riemann zeta function by Artin and Mazur [44].

[8] This definition (see for instance [45]) is not the standard definition mathematicians are used to, namely a topological entropy defined for a continuous transformation of a compact set. However, since we are not interested in flows but rather in discrete maps we prefer to take a definition for the topological entropy in terms of the rate of growth of periodic points. The paper by Friedland [50] gives a definition of the topological entropy for a rational map. For the Hénon family of maps, the topological entropy does coincide with (12) (see Lemma 2 of [19]). A paper by Favre [29] gives a good idea of a precise counting of periodic points for birational maps in the complex plane.

$$\log h = \lim_{N\to\infty} \frac{\log(\#\mathrm{fix}(k^N))}{N}. \tag{12}$$

If the dynamical zeta function is a rational expression in t, then h will be the inverse of the pole of smallest modulus of $H(t)$ or $\zeta(t)$. Since the number of fixed points remains unchanged under topological conjugacy (see [51] for this notion), the dynamical zeta function is thus a topologically invariant function, i.e. invariant under a large set of transformations: it does not depend on a specific choice of variables.

In the case of mapping (1) and for generic values [9] of ϵ, the expansion of $H_\epsilon(t)$ coincides [10] with one of the rational function

$$H_\epsilon(t) = \frac{t(1+t^2)}{(1-t^2)(1-t-t^2)}, \tag{13}$$

which corresponds to a very simple rational expression for the dynamical zeta function

$$\zeta_\epsilon(t) = \frac{1-t^2}{1-t-t^2}. \tag{14}$$

It has been conjectured in [33] that *the simple rational expression* (14) *is the actual expression of the dynamical zeta function for any generic value of* ϵ (up to some algebraic values of ϵ, like (26) or (27), where one obtains another expression [35] but with the same singularity $1-t-t^2$). Similar calculations have been performed for the other non-generic values of ϵ that have been singled-out in the semi-numerical analysis [35]. For example, for the non-generic values of ϵ, $\epsilon = 1/m$ with $m \ge 4$, we have obtained expansions [33–35] compatible with the following rational expression:

$$\zeta_{1/m}(t) = \frac{1-t^2}{1-t-t^2+t^{m+2}} \tag{15}$$

giving a topological entropy smaller than the generic one ($h \simeq 1.6108$).

2.3. Arnold complexity

Another topological measure of complexity has been introduced for two-dimensional discrete dynamical systems, namely the Arnold complexity [6]. The Arnold complexity amounts to counting the number of complex intersections of a given (complex projective) line [11] with its Nth iterate under a given transformation. It can be shown that (generically [12]) this number is independent of the chosen (complex) line, and, of course, it is independent of the variables used to describe the transformation. The Arnold complexity is thus, also, a topological invariant [6]. Since such topological invariances are noticed for the Arnold complexity [36], as well as for the topological entropy, it is thus tempting to make a connection between the rationality of the Arnold complexity generating function (to be given below), and the rationality of the dynamical zeta function (if any, etc.). We have also compared the singularities of these two sets of generating functions, namely the growth complexity λ, and h, the (exponential of the) topological entropy [33].

In general, for a rational transformation the Arnold complexity A_N corresponding to N iterations *grows exponentially* with N : $A_N \simeq \lambda^N$. The iteration of rational transformations yields larger and larger rational expressions,

[9] Namely $\epsilon \ne 1/m (m \ge 1)$ or $\epsilon \ne (m-1)/(m+3)$ with m odd and, possibly, ϵ different from a set of algebraic values like (26) or (27).
[10] We do not count here the fixed point at infinity [35].
[11] In fact, this can even be generalized to counting the number of (complex) intersections of a fixed (algebraic) curve with its Nth iterate.
[12] For instance, there may exist singled-out lines which are globally invariant under the transformation one iterates. In that case, the number of Arnold intersections of the line with its Nth iterate is infinite. The line $y = z + 1$ is such an example.

at each iteration step, and it is simple to see that the degrees of the numerators (or denominators) of these rational expressions also grow exponentially like $\simeq \lambda^N$, where λ is actually the same as the previous λ related to the Arnold complexity [6]. One can, of course, introduce generating functions corresponding to these successive Arnold complexities A_N, or of these successive degrees

$$A(t) = \sum_{N=1}^{\infty} A_N t^N. \tag{16}$$

For the birational transformation (1), one finds, respectively, for generic values of ϵ, and for non-generic values of the form $\epsilon = 1/m$:

$$A_\epsilon(t) = \frac{t}{1-t-t^2}, \qquad A_{\epsilon=1/m}(t) = \frac{t}{1-t-t^2+t^{m+2}}. \tag{17}$$

On these exact rational expressions (17), one sees that the value of λ, associated with the Arnold complexity (or, equivalently, with the growth of the degree of the successive rational expressions in the iterations), actually identifies with h, the exponential of the topological entropy (see (14) and (15)). The possible identification of these two topological complexities has been discussed in detail in previous publications [33–35]. This identification has also been verified on a few other two-dimensional birational *measure-preserving* transformations generated by involutions. It is, however, not clear to figure out if this identification actually holds for all the birational transformations generated by involutions, or all the measure-preserving maps (see Section 2.4).

2.4. Some comments on the relations between various entropies and complexity measures

One should recall that upper estimations for the topological entropy [52], as well as relations between degree complexity and topological entropy are discussed in the literature (see, e.g. [53] but only for C^1 maps). We do not want to mention here the well-known inequalities between the metric entropy and the topological entropy, or even the more general order-q Renyi entropies [54]. We just want, here, to look at the relations between two *topological* complexities, namely the topological entropy and Arnold complexity, and in the following, their real adaptations. In this respect, one must certainly mention the relations and inequalities given by Newhouse [55] relating the topological entropy of a smooth map to the growth rates of the volumes of iterates of smooth manifolds.[13] For C^∞-smooth mappings, Yomdin [57,58] proved the opposite inequality, thus showing the coincidence of the growth rate of volumes and topological entropy. One should also recall the paper by Friedland [50] which shows that the entropy is the same as the volume growth for rational self-maps of complex projective space P^2: in that case, the Arnold complexity coincides with the growth of homology [59] which should be the same as the volume growth.

In fact, it is not completely clear to see if one can actually use all these mathematical theorems for our birational measure-preserving mappings. When mathematicians study birational transformations they tend to focus on the indeterminacy set where a birational map cannot be defined and are very worried about the bad things that might arise when this set grows with the iteration. In order to avoid such mathematically unpleasant proliferation of singularities, they work in a framework which is a very smooth one with a point of departure of diffeomorphisms. The conceptual framework, and even the definitions of the topological entropy, being slightly different, it is difficult to see if these theorems really apply. Let us just point here that, fortunately, the indeterminacy locus is far from being a dense set: it is very tame for mappings (1).

From a more down-to-earth point of view, the comparison between topological entropy and Arnold complexity can be understood as follows. The components of $k_\epsilon^N(y,z)$, namely y_N and z_N, are of the form $P_N(y,z)/Q_N(y,z)$ and

[13] Schub [56] conjectured that the topological entropy of a smooth map on a compact manifold is bounded by the growth of the various algebraic transformations that it induces.

$R_N(y,z)/S_N(y,z)$, where $P_N(y,z)$, $Q_N(y,z)$, $R_N(y,z)$ and $S_N(y,z)$ are polynomials of degree asymptotically growing like λ^N. The Arnold complexity amounts to taking the intersection of the Nth iterate of a line (for instance a simple line like $y = y_0$, where y_0 is a constant) with another simple (fixed) line (for instance $y = y_0$ itself or any other simple line or any fixed algebraic curve). For instance, let us consider the Nth iterate of the $y = y_0$ line, which can be parameterized as

$$y_N = \frac{P_N(y_0,z)}{Q_N(y_0,z)}, \qquad z_N = \frac{R_N(y_0,z)}{S_N(y_0,z)}, \tag{18}$$

with line $y = y_0$ itself. The number of intersections, which are the solutions of $P_N(y_0,z)/Q_N(y_0,z) = y_0$, grows like the degree of $P_N(y_0,z) - Q_N(y_0,z)y_0$: asymptotically it grows like $\simeq \lambda^N$. On the other hand, the calculation of the topological entropy corresponds to the evaluation of the number of fixed points of k^N, i.e. the number of intersections of the two curves: $P_N(y,z) - Q_N(y,z)y = 0$ and $R_N(y,z) - S_N(y,z)z = 0$ which are two curves of degree growing asymptotically like $\simeq \lambda^N$. The number of fixed points is obviously bounded by $\simeq \lambda^{2N}$. The exponential of the topological entropy, namely h, is thus bounded by the square of $\lambda : h \le \lambda^2$.

In fact, we have found a possible example where this upper bound seems actually to be reached. Let us consider the quadratic transformation

$$(y,z) \to ((A - y - Bz)y, (A - Cy - z)z). \tag{19}$$

The mapping is not bipolynomial or birational. The dynamical zeta function reads (up to order 5 only, the calculations now become really large, etc.) for this non-invertible mapping

$$\zeta(t) = \frac{1}{(1-t)^4(1-t^2)^5(1-t^3)^{20}(1-t^4)^{60}(1-t^5)^{204}} \cdots \tag{20}$$

from which one can conjecture that

$$\zeta(t) = \frac{1-t^2}{1-4t}. \tag{21}$$

This provides an example for which $h = \lambda^2 = 4$. Therefore, it seems that the identification of h and λ is not valid in general. [14] It seems that the identification of h and λ might be related to the "very tame" proliferation of singularities of the (birational) transformations (1), or it might be a consequence of the measure-preserving property of the mapping. This is a quite complicated analysis that we do not want to sketch here. Let us just say that this identification seems to be a valid one in our particular example (1).

2.5. Real topological entropy

The previous definitions of the dynamical zeta functions $\zeta_\epsilon(t)$, and of the generating function $H_\epsilon(t)$ counting the number of fixed points, can be straightforwardly modified to describe the counting of real fixed points:

$$H_{\mathrm{real}}(t) = \sum_N H_N^R t^N = t\frac{\mathrm{d}}{\mathrm{d}t}\log(\zeta^{\mathrm{real}}(t)), \quad \zeta^{\mathrm{real}}(t) = \sum_N z_N^R t^N, \tag{22}$$

where the number of real fixed points H_N^R also grows exponentially with the number N of iterates, like $\simeq h_{\mathrm{real}}^N$. A quick examination of phase portraits associated with various generic values of the parameter ϵ on one side, and of the corresponding visual complexities on the other side [37], shows an agreement with the corresponding value for h_{real}.

[14] One can imagine that some equality like $h = \lambda h_{\mathrm{sing}}$ could be valid, where h_{sing} could correspond to the exponential proliferation of bifurcations or singularities. Such speculative ideas remain to be studied.

These real dynamical zeta functions have been extensively analyzed in [37] for various values of ϵ. Let us just recall here some remarkable results for particular values of ϵ. Actually for $\epsilon = 3$, the real dynamical zeta function is very simple. One only has a single real fixed point for k_ϵ^N, namely the fixed point of k_ϵ, and thus $\zeta_\epsilon^{\rm real}(t)$ identifies with a very simple rational expression:

$$\zeta_{\epsilon=3}^{\rm real}(t) = \frac{1}{1-t}, \qquad H_{\epsilon=3}(t) = \frac{t}{1-t}. \tag{23}$$

Furthermore, let us specify the value $\epsilon = \frac{21}{25}$ for which the real dynamical zeta function $\zeta_\epsilon^{\rm real}(t)$ seems to identify, up to the order for which its series expansion has been calculated,[15] with a simple rational expression [37]:

$$\zeta_{21/25}^{\rm real}(t) = \frac{1+t^2}{1-t+t^2-2t^3}, \qquad H_{21/25}^{\rm real}(t) = \frac{t(1+2t^4+5t^2)}{(1+t^2)(1-t+t^2-2t^3)}. \tag{24}$$

For ϵ large enough, one also gets [37] a remarkably simple rational expression

$$\zeta_{\epsilon=\infty}^{\rm real}(t) = \frac{1+t}{1-t^2-t^3-t^5} = \frac{1-t^2}{(1-t-t^2)+t^4(1-t+t^2)} \tag{25}$$

yielding an algebraic value for $h_{\rm real}$: $h_{\rm real} \simeq 1.4291$. It is not clear whether this rationality property holds for any value of ϵ.

2.6. Real Arnold complexity

Similarly, recalling the Arnold complexity [6] which counts the number of intersections between a fixed (complex projective) line and its Nth iterate [6], and the associated Arnold generating functions (16), one can slightly modify these definitions to describe discrete dynamical systems bearing on real variables. For this, let us now count the number of real points which are the intersections between a given real fixed line and its Nth iterate. We have actually calculated these real Arnold complexities for various values of ϵ, and for various given (real) lines. All these calculations have been cross-checked by a (maple) program calculating these numbers of intersections using the Sturm procedure in maple.[16] Let us denote by $\mathcal{A}_N$ the number of these (real) intersections for the Nth iterate. It is clear that these real Arnold complexities, $\mathcal{A}_N$, are not as universal as the standard Arnold complexities which are basically a degree counting: the $\mathcal{A}_N$'s depend on the given (real) line one iterates. However, one can expect, in the large N limit, that $\mathcal{A}_N$ will grow exponentially like $\simeq \lambda_{\rm real}^N$, $\lambda_{\rm real}$ being independent of the (generic) line one iterates. Indeed, this has been checked for various lines and we have found for the birational transformation (1), that the singled-out line $y = \frac{1}{2}(1-\epsilon)$ is well suited to get quite regular, and long enough, series for the $\mathcal{A}_N$'s (see [37]). We will denote as $\mathcal{A}_\epsilon(t)$ the generating function of these $\mathcal{A}_N$'s.

In order to estimate a real growth complexity $\lambda_{\rm real}$, we have calculated $\mathcal{A}_N^{1/N}$, for various values of the number of iterations ($N = 13, 14, 15$), as a function of ϵ, in the range $[0, 1]$ where $\lambda_{\rm real}$ has a quite rich behavior [37]. Let us show here an estimation of $\lambda_{\rm real}$ by $\mathcal{A}_{13}^{1/13}$, as a function of the parameter ϵ, in the interval $[-0.1, 3.1]$.

[15] In fact, up to the order for which the series expansions have been calculated, it seems that $\zeta_\epsilon^{\rm real}(t)$ remains associated with the same series expansions for ϵ in some interval like $\simeq [\frac{21}{25}, \frac{24}{25}]$. This deserves further study.

[16] The Sturm procedure one can find in maple gives the number of real roots of a polynomial in any interval $[a, b]$, even for the interval $]-\infty, +\infty[$. The Sturm procedure uses Sturm's theorem [60] to return the number of real roots of polynomial P in the interval $[a, b]$. The first argument of this Sturm procedure is a Sturm sequence for P, which can be obtained with another procedure, the procedure Sturmseq which returns the Sturm sequence as a list of polynomials and replaces multiple roots by single roots.

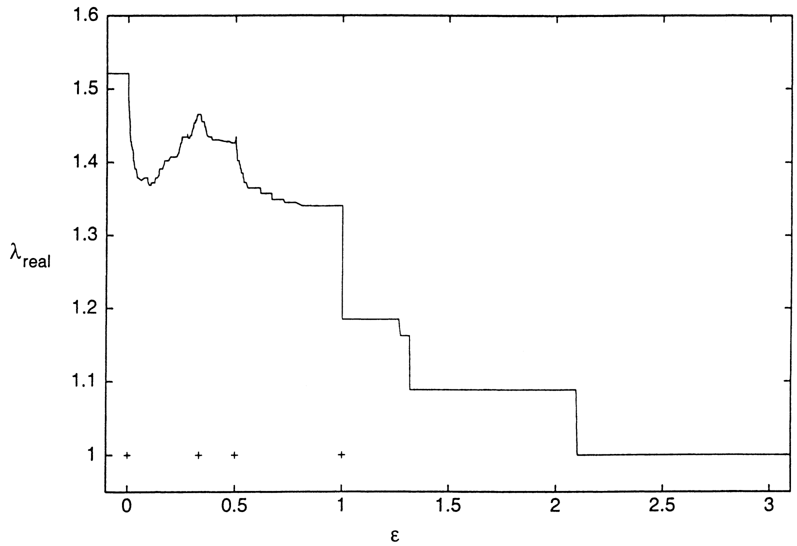

Fig. 1. An estimation of λ_{real} by $\mathcal{A}_{13}^{1/13}$, as a function of the parameter ϵ, in the interval $[-0.1, 3.1]$. The integrable points $\epsilon = -1, 0, \frac{1}{3}, \frac{1}{2}, 1$ are represented by crosses.

Fig. 1 shows that λ_{real}, as a function of ϵ, looks like a continuous [17] function. In fact, it can be shown [37] that $\mathcal{A}_{13}^{1/13}$ (and more generally $\mathcal{A}_N^{1/N}$ for any finite integer N) is actually a staircase function, the limits of each "interval-step" of the staircase being remarkable algebraic numbers. These algebraic values are distributed in various families of values of ϵ. The simplest family of singled-out algebraic values of ϵ corresponds to the fusion on an N-cycle with the 1-cycle, and reads [35,61]

$$\epsilon = \frac{1 - \cos(2\pi M/N)}{1 + \cos(2\pi M/N)} \quad \text{or equivalently} \quad \cos\left(2\pi \frac{M}{N}\right) = \frac{1-\epsilon}{1+\epsilon} \tag{26}$$

for any integer N (with $1 < M < \frac{1}{2}N$, M not a divisor of N). Other cycle-fusion mechanisms [61] take place yielding new families of algebraic values for ϵ. For instance, the coalescence of the $(3 \times N)$-cycles in the 3-cycle, and the coalescence of the $(4 \times N)$-cycles in the 4-cycle yield, respectively (with some constraints on the integer M that will not be detailed here [61]),

$$\cos\left(2\pi \frac{M}{N}\right) = 1 - \frac{3}{4}\frac{\epsilon(\epsilon-3)^2}{(1-\epsilon)(1+\epsilon)}, \qquad \cos\left(2\pi \frac{M}{N}\right) = 1 - 32\frac{\epsilon(1-\epsilon)^2}{(1+\epsilon)^2(1-2\epsilon)}. \tag{27}$$

The real complexity λ_{real} is the large N limit of these staircase functions $\mathcal{A}_N^{1/N}$, thus taking into account all these families of algebraic values. It is, however, not clear to figure out if this limit will be a continuous function of ϵ (up to the non-generic values of ϵ, $\epsilon = 1/m \ldots$), like Fig. 1 would suggest at first sight, or if it will be more a "devil's staircase" function of ϵ. These calculations have been extensively displayed in [37]. Let us just recall here a set of

[17] One should note that λ_{real} takes smaller discontinuous values on the (infinite) discrete set of values of ϵ which is the union of the set of integrable values of ϵ, together with the two (infinite) discrete sets of non-generic values of ϵ previously mentioned ($1/m$ with $m \geq 4$ and $(m-1)/(m+3)$ with $m \geq 7$, m odd). All these values must be treated separately. The integrable points $\epsilon = -1, 0, \frac{1}{3}, \frac{1}{2}, 1$ are represented by crosses in Fig. 1.

values of ϵ corresponding to remarkable expressions for $\mathcal{A}_\epsilon(t)$. First, for $\epsilon = 3$, one obtains

$$\mathcal{A}_3(t) = \frac{t}{1-t}, \tag{28}$$

which is in perfect agreement with the expression of the real dynamical zeta function $\zeta_{\epsilon=3}^{\text{real}}(t)$ (see (23)). Another value of ϵ seems to yield an exact rational expression for the real Arnold generating function $\mathcal{A}_\epsilon(t)$, namely $\epsilon = \frac{21}{25}$:

$$\mathcal{A}_{21/25}(t) = \frac{t(1+t+t^2+t^3-2t^4)}{(1-t)(1+t)^2(1-t+t^2-2t^3)}, \tag{29}$$

which is also in agreement with the real dynamical zeta function (24) with the same singularities. Finally, it is also worth recalling the large ϵ limit, where, again, one gets a simple rational expression for the real Arnold generating function, namely

$$\mathcal{A}_\infty(t) = \frac{t(1+t^4)}{(1-t^2-t^3-t^5)(1-t)} = \frac{t(1+t^4)}{(1-t-t^2)+t^4(1-t+t^2)}. \tag{30}$$

All the results, displayed in this section and in [37], seem to show, again, that the identification between h_{real} and λ_{real} could actually hold [37] for mapping (1). However, in contrast with the universal behavior of the usual Arnold complexity, or topological entropy, displayed in Fig. 1, λ_{real} and h_{real} are quite involved functions of the parameter ϵ (see Fig. 1).

3. From (real) topological complexity towards metric complexity and Lyapunov characteristic exponents

The real topological entropy or λ_{real} associated with the real Arnold complexity are well-suited evaluations of the visual complexity as it can be seen [37] on the phase portraits of transformation (1). Coming from an ergodic, or probabilistic, or (real) functional analysis approach of dynamical systems, one may have the prejudice that coping with real analysis (instead of complex projective analysis) could yield to lose most of the universality properties. To some extent, dealing with mappings bearing on real variables, we have actually lost most of the topological universality (Smale's invariance [51]), but it is clear on some remarkable algebraic results, like (25) or (30) for instance, that some underlying algebraic structure still remains. [18] Apparently, notions like the two previous (and possibly redundant for mapping (1)) notions of real topological entropy and real Arnold complexity seem to fill "a little bit" the well-known (huge) gap existing, in the study of dynamical systems, between the topological approach and the probabilistic approach [19] [62]. In the framework of real analysis, the "probabilistic" approach has created many concepts in order to describe, and better understand, the complexity of dynamical systems (Lyapunov dimension, or Kaplan–Yorke dimension [63], fractal dimensions of some strange attractor, if any, etc. Renyi's q-entropies [64], Lyapunov characteristic exponents [65,66], Kolmogorov–Sinai metric entropy [38,39], etc.). These various notions concentrate on different aspects of the complexity of dynamical systems (sensitivity to initial conditions, complexity of some natural geometrical objects like strange attractors, difficulty to go backwards in the iteration process, "loss of memory", etc.). Among these various notions some are quite "model-dependent", depending on many specific details, others are more interesting since they can be used to describe larger classes of dynamical systems.

[18] For instance, one could imagine to introduce a notion of real Smale's invariance corresponding to all the conjugacies (change of variables) preserving $\zeta_\epsilon^{\text{real}}(t)$ or $\mathcal{A}_\epsilon(t)$.

[19] Or, as mathematicians say, between the topological category and the measure category.

In this respect, the Kolmogorov–Sinai metric entropy [38] is an interesting notion, since it takes into account "some structure", namely the metric structure. [20] Furthermore, it has a quite large set of invariances, the measure-preserving conjugacies. Similarly, the real topological entropy does not have the very large Smale's topological invariance [51] of the standard topological entropy, but exact algebraic results like (25), seem to indicate that there actually also exists a large enough set of invariances for this new concept. Therefore, the Kolmogorov–Sinai metric entropy is, on the probabilistic side, a quite good "candidate" in order to be compared with our two real and topological concepts (namely the real topological entropy and the real Arnold complexity). The metric entropy is probably, among the various notions belonging to the probabilistic approach, the concept which is the "closest" to the real topological entropy concept. Naively, on the specific example of the birational transformation (1), one would like to see if the real topological entropy could be seen as some kind of "improved" metric entropy taking into account all the metric (measure) description, and real analysis description, performed by the metric entropy, but providing more than non-effective results of probabilistic theory and actually, from time to time, exact results.

Fig. 1 has been obtained using the Sturm's theorem [60] which enables to get the number of real intersections of a line with its Nth iterate independently of the actual localizations [21] of these intersection points: Sturm's theorem is a very efficient tool in order to just get this number of (real) intersections which was actually the (topological) information we were looking at. Of course, if one tries to get less topological and more metric informations, like the actual localizations of these intersections, or the distances between these intersections, the calculations become much more time consuming. Actually, we have also performed such "time consuming" calculations, trying to get some hint on the actual localization of these intersections. We found, for some values of ϵ, that many intersection points can be localized at a quite large distance from the origin, i.e. out of the frame of a phase portrait (like Fig. 4). Furthermore, one also finds (for 13, 14 or 15 iterations) that many of these intersection points can get extremely close from each other for some values of ϵ, and that it becomes necessary to perform calculations with a precision of more than 4000 digits. With a smaller precision, one gets smaller numbers of intersections since one is not able to "discriminate" between some intersection points. The "visual complexity", as it can be seen in Fig. 4, and as it is described in Fig. 30 (see Appendix A), takes into account intersection points inside a given frame and for a given precision (corresponding to the minimal distance between two points "our eyes" can discriminate). Actually, one can calculate a "modified" Arnold complexity, $\tilde{A}_N$, corresponding to a calculation with a finite, not too large, precision (e.g. 1000 digits, etc.) and to intersection counting in some finite box, and thus corresponding more to the "visual complexity", as it can be seen on the phase portraits. Of course, one can also calculate $\tilde{A}_N^{1/N}$ which is supposed to have a large N limit. This introduces a "less universal" (more metric), scale-dependent, notion of (real Arnold) complexity. Some details are given in Appendix A. Of course, there are many (not very well-defined, etc.) ways to change the real topological entropy, or the real Arnold complexity, into a less universal quantity turning it into a more metric quantity, which tries to "fill the gap" between the metric point of view and the topological point of view. We do not want to add more confusion. Therefore, on the specific example (1) and for various values of ϵ, we will just restrict ourselves to a comparison between two well-defined notions: the real topological entropy [37] (or equivalently λ_{real}) and the metric entropy [38].

The definition of the Kolmogorov–Sinai metric entropy being "not very effective" [3,4], let us recall Pesin's formula [68], which gives the metric entropy as an integral of the Lyapunov characteristic exponents $\ln(\lambda)^+$, but is

[20] The "metric entropy" of a measure is a property of the invariant measure. It is invariant under measure-preserving transformations, which have no relations with the metric property of the space. Therefore, the terminology "metric entropy" might seem misleading from a linguistic point of view. This is, however, the terminology physicists are used too.

[21] Concerning the geometric location of intersection points one can cite the paper by Bedford et al. [67] where it is shown, in the framework of polynomial diffeomorphisms of C^2 that there is a convergence of measures of the asymptotic location of the intersection points to the invariant measure.

only valid in the framework of hyperbolic systems:

$$S_{\text{metric}} = \int \mathrm{d}\mu \, \ln(\lambda)^{+}, \tag{31}$$

where $\mathrm{d}\mu$ denotes the invariant measure of the transformation.[22] Unfortunately, transformation (1) does not correspond to a hyperbolic system: it is a measure-preserving map. Pesin's formula which is valid in a hyperbolic framework can thus only be considered as a possible evaluation of the metric entropy. Furthermore, any effective calculation of the invariant measure is extremely difficult to be performed. Alternatively, one can also recall [69] the Pesin inequality:[23]

$$\sum_{\lambda_i \geq 0} \lambda_i \geq h_{\mathrm{d}\mu}(f), \tag{32}$$

where $\mathrm{d}\mu$ denotes an invariant measure, λ_i denotes the set of Lyapunov exponents with respect to $\mathrm{d}\mu$, and $h_{\mathrm{d}\mu}$ the metric entropy of $\mathrm{d}\mu$. The Pesin inequality[24] shows that whenever the Lyapunov exponents are zero, the metric entropy is also zero.

Since we are not really able to actually calculate the metric entropy for our non-hyperbolic measure-preserving transformation (1); we will calculate, instead of the metric entropy, as many Lyapunov characteristic exponents as possible, as a function of the parameter ϵ.

4. Phase portraits and Lyapunov characteristic exponents

Therefore, in order to fill the gap between the probabilistic point of view and the topological point of view on this specific birational example, we will try to compare Lyapunov characteristic exponents with the real topological entropy, or, in practice, λ_{real} associated with the real Arnold complexity, which is much easier to evaluate, for the birational transformation (1).

4.1. An infinite precision program to calculate the Lyapunov characteristic exponents

The calculations of the Lyapunov characteristic exponents have been performed using an infinite-precision[25] C-library.[26] Let us briefly sketch the program calculating the Lyapunov characteristic exponents.

At each iteration step, we calculate for a given initial point (y, z), the Jacobian matrix of transformation k_ϵ^N as the product of the previous Jacobian matrices of transformations k_ϵ^M (evaluated at the same point), where $M \leq N - 1$:

$$J_{\text{ac}}[k_\epsilon^N](y,z) = J_{\text{ac}}[k_\epsilon](k_\epsilon^{N-1}(y,z)) \cdots J_{\text{ac}}[k_\epsilon](k_\epsilon^3(y,z))\, J_{\text{ac}}[k_\epsilon](k_\epsilon^2(y,z))\, J_{\text{ac}}[k_\epsilon](k_\epsilon(y,z))\, J_{\text{ac}}[k_\epsilon](y,z) \tag{33}$$

and calculate the two eigenvalues of this Jacobian matrix, $\lambda_1^{(N)}$ and $\lambda_2^{(N)}$. Finally, we take the logarithm of the

[22] Our birational transformation can be seen to be the product of two involutions [31]. There actually exist some theorems showing that a mapping, product of two involutions, has necessarily an invariant measure. However, transformation (1) is not a hyperbolic system. In the case of real mappings, like k_ϵ is seen in a large part of our paper, it would be interesting to know when these measures (defined a priori on C^2) are in fact measures on R^2. This question was answered for the Hénon family [67].

[23] The hypothesis for this theorem is that f is a smooth function of class C^1.

[24] There is also a generalization of Pesin's inequality valid for any Borel measure which is ergodic and hyperbolic [70].

[25] The multi-precision library gmp (GNU MP) is part of the GNU project. It is a library for arbitrary precision arithmetic, operating on signed integers, rational numbers and floating points numbers. It is designed to be as fast as possible both for small and huge operands. The current version is 2.0.2. Targeted platforms and software/hardware requirements are any Unix machines, DOS and others, with an operating system with reasonable include files and a C compiler.

[26] Information on the multi-precision library gmp (GNU MP) can be found at the following: Home site: http://www.nada.kth.se/tege/gmp/; other links: ftp://prep.ai.mit.edu/pub/gnu/(gmp-*.tar.gz); mailing lists/USENET; news groups: bug-gmp@prep.ai.mit.edu.

modulus of these two eigenvalues divided by the number N of iterations

$$L_1^{(N)} = \frac{\ln(|\lambda_1^{(N)}|)}{N}, \qquad L_2^{(N)} = \frac{\ln(|\lambda_2^{(N)}|)}{N}. \tag{34}$$

When the two previous quantities, $L_1^{(N)}$ and $L_2^{(N)}$, tend to some finite limits [27] in the large N limit, one can define a Lyapunov characteristic exponent which will be the largest of these two limits. For an integrable mapping, these two limits can be drastically different (see Fig. 3 (left)), while for a more “chaotic” orbit, the two previous numbers are very much on the same footing, being quite close. In fact, in more chaotic situations, it is difficult to make a relevant distinction, valid for any N, between $L_1^{(N)}$ and $L_2^{(N)}$. Therefore, in the following, we will often plot both quantities, as a function of N, at the same time. Our program also calculates the determinant of the Jacobian matrix $J_{\mathrm{ac}}[k_\epsilon^N](y, z)$. This program also uses extensively the reversible character of the birational transformation (1). Actually, we use the fact that the inverse transformation, k_ϵ^{-1}, is a simple rational transformation to go backwards to the initial point (y, z). Due to the finite numerical precision, one does not come back exactly to the initial point (y, z), and one can thus compare the distance between this one-way and return point and the initial point. If this distance is not small enough we increase the precision in our infinite-precision program. Typically, for 5×10^5 iterations a calculation performed with precision of 1×10^{-240} can give a numerical deviation of 1×10^{-100} when one returns to the initial point using the inverse rational transformation k_ϵ^{-1}. In other words, we can trust our calculations, namely the $L_i^{(N)}$'s, and the points of the orbit obtained this way, up to $\simeq 1 \times 10^{-100}$. If one goes on iterating, this numerical deviation goes on deteriorating: after 2×10^5 more iterations the deviation to the initial point can be of the order of 1×10^{-30}. This is just an example. In fact, this deterioration is highly sensitive to the transformation one considers (here the parameter ϵ) and especially the orbit one considers. Our program is built in such a way that one increases the precision as much as necessary in order to have a deviation smaller than 1×10^{-30} when one performs the iterations and goes back to the initial point using the inverse transformation. In fact, for most of the calculations performed here the deviation is smaller than 1×10^{-100}. In the following, the most difficult situation will correspond to some analysis near the point at infinity, for which a precision of 8000 digits is necessary in order to have a deviation smaller than 1×10^{-30} when one performs 5×10^6 iterations and goes back to the initial point. Let us remark that our calculations correspond to the actual definition of the Lyapunov characteristic exponents [65]: it is a quantity associated to a single orbit, we are not averaging over some set of orbits corresponding to some neighborhood of the initial point.

4.2. Checking the infinite precision program

In order to check the results of our infinite-precision program, we have used it on three different kinds of birational transformations: the well-known Hénon map [18,19], several two-dimensional collineation transformations, and mapping (1) for integrable values of ϵ. Let us just detail here the Lyapunov calculations corresponding to the integrable values of ϵ of mapping (1). Mapping (1) is known to be integrable for various values of ϵ, namely $\epsilon = -1, 0, \frac{1}{3}, \frac{1}{2}, 1$ (see [32]). For $\epsilon = \frac{1}{2}$, one gets a linear pencil of elliptic curves, namely (ρ denotes a constant)

$$\Delta(y, z, \tfrac{1}{2}) = \frac{(1 + z + 2yz)(1 - y + 2yz)(1 + z - y - 2yz)}{(1 + z - y)^2} = \rho. \tag{35}$$

The calculations of the Lyapunov characteristic exponents, performed with our program, clearly indicate Lyapunov characteristic exponents equal to zero. One has a similar situation for most of the other integrable values for which the accumulation of the infinite set of points is dense in the integrable, elliptic or rational, algebraic curves. In order

[27] For instance, the assumptions of the Oseledec’s theorem [71] ensure a reasonably linear-friendly environment yielding the two previous quantities, $L_1^{(N)}$ and $L_2^{(N)}$, to have some limits when N gets large.

to get some non-trivial non-zero values for the limits of the $L_i^{(N)}$'s, let us consider mapping (1) for the integrable value $\epsilon = 0$. For $\epsilon = 0$, it is straightforward to see that the orbits correspond to a foliation of the (y, z)-plane into rational curves, namely the very simple hyperbola

$$\Delta(y, z, 0) = yz = \rho. \tag{36}$$

Using this rational foliation, one can rewrite transformation (1) as a simple homographic transformation on a single variable, namely y, with two fixed points $y_\pm$

$$y \to 1 + \frac{\rho}{y}, \qquad y_\pm = \tfrac{1}{2}(1 \pm (1 + 4\rho)^{1/2}), \tag{37}$$

which enables to rewrite the homographic transformation (37) as

$$\frac{y - y_+}{y - y_-} \to \lambda \frac{y - y_+}{y - y_-}, \quad \lambda = \frac{y_-}{y_+} = \frac{1 - (1 + 4\rho)^{1/2}}{1 + (1 + 4\rho)^{1/2}}. \tag{38}$$

For $\rho < -\frac{1}{4}$, one finds out that λ is on the unit circle: $\lambda = \mathrm{e}^{-2\mathrm{i}\theta}$, where the angle θ is such that $(\tan\theta)^2 = -1 - 4\rho$. For $\rho > -\frac{1}{4}$, one has an exponentially fast convergence to one of the two fixed points (37). Therefore, hyperbola $yz = -\frac{1}{4}$ is a frontier, in the phase portrait, between a region of the (y, z)-plane where the infinite set of points of an iteration form a set of points dense in the $yz = \rho = y_0 z_0$ hyperbola (corresponding to the iteration of the initial point (y_0, z_0)), and another region, $yz > -\frac{1}{4}$, where all the orbits of an initial point (y_0, z_0) converge exponentially fast (along the $yz = y_0 z_0$ hyperbola) to fixed points, like (37), where $\rho = y_0 z_0$. This partition of the (y, z)-plane into two regions, an ergodic region, and a region of exponentially fast convergence, is well illustrated on the phase portrait for $\epsilon = 0$.

In the $yz > -\frac{1}{4}$ region of "exponentially fast convergence" to fixed points of Fig. 2, "the initial points (numbering 70)" have been chosen randomly. One sees an accumulation of points on the line $y = 1 + z$, which corresponds exactly to the elimination of ρ between $y_\pm = \frac{1}{2}(1 \pm (1 + 4\rho)^{1/2})$ (see (37)) and $z_\pm = \rho / y_\pm$. In the $yz < -\frac{1}{4}$ ergodic region of Fig. 2, the Lyapunov's calculations, performed with our program, give Lyapunov characteristic exponents equal to zero, while in the region of exponentially fast convergence to fixed points of Fig. 2, one gets non-trivial negative values for the limits of the $L_i^{(N)}$'s, in perfect agreement with the exact values which should, of course, be

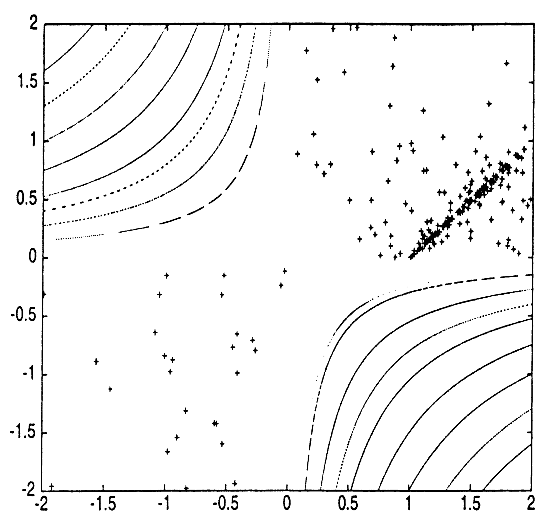

Fig. 2. Phase portrait for $\epsilon = 0$ in the (y, z) variables.

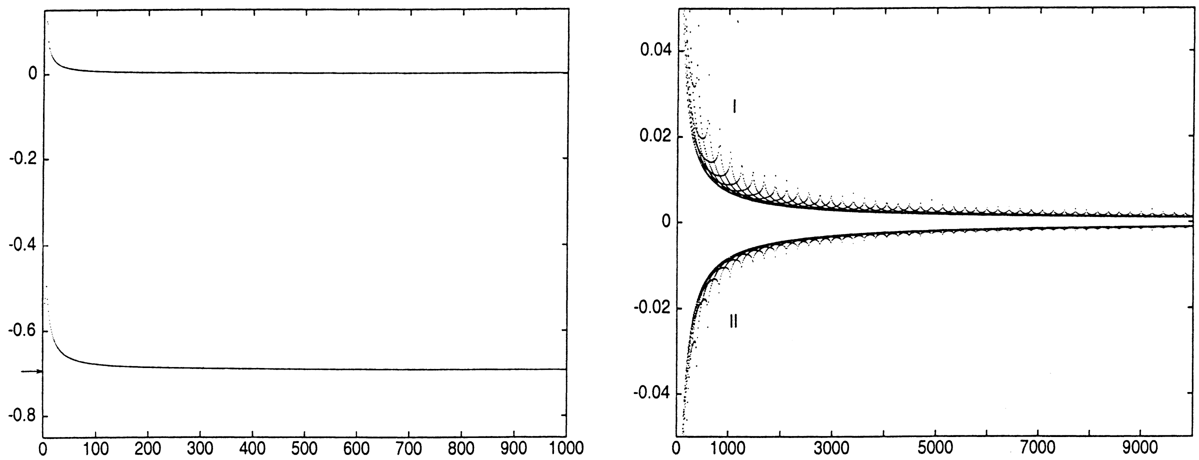

Fig. 3. $L_1^{(N)}$ and $L_2^{(N)}$, as a function of N, for an orbit in the region of exponentially fast convergence of Fig. 2, namely $\rho = y_0 z_0 = 2$ (left) versus an ergodic situation, namely $\rho = y_0 z_0 = -2$ (right).

$$L_{\text{yap}} = \ln(|\lambda|) = \ln\left(\left|\frac{1 + 2\rho - (1 + 4\rho)^{1/2}}{2\rho}\right|\right), \tag{39}$$

where λ is given by (38). Let us take an initial point (y_0, z_0) such that $\rho = y_0 z_0 = 2$. This value of ρ is chosen such that the previous expression becomes simple, namely $L_{\text{yap}} = \ln \frac{1}{2}$. Let us just give, here, $L_1^{(N)}$ and $L_2^{(N)}$, as a function of N, for an orbit of an initial point (y_0, z_0) in the region of exponentially fast convergence for $\rho = y_0 z_0 = 2$, and compare it with an ergodic situation corresponding to $\rho = y_0 z_0 = -2$.

One does see in Fig. 3 (left) that one has two quite different values $L_1^{(N)}$ and $L_2^{(N)}$: one value goes, very quickly, to zero (as it should), and the other one converges very quickly to the asymptotic exact negative value $\ln \frac{1}{2}$. In the ergodic case, $L_1^{(N)}$ and $L_2^{(N)}$ quickly converge to a zero value.

Remark (The integrable situation in elliptic regions). *The zero Lyapunov results in all the* (*integrable*) *ergodic regions, where one gets an infinite set of points dense in the algebraic curves, can, heuristically, be easily understood as follows: the movement on these regular orbits can be thought, in some well-suited variable* θ, *as a simple shift* $\theta \to \theta + \lambda$, *the iteration being* (*in the real phase space*) *isomorphic to a rotation on the unit circle* (*with an angle not generically commensurate with* 2π). *The distance between two very close points on these curves is constant in the well-suited variable* θ, *and, in the plain variables y and z, is a periodic function* $P(\theta)$. *This distance between the Nth iterates of two neighboring points of the initial point* (y, z), *can be written, as a function of N, as* $P(\theta_0 + N\lambda)$, *where* θ_0 *corresponds to the initial point* (y, z). *The Lyapunov's calculations amount to trying to see the previous expression as* $\exp(NL_{\text{yap}})$: *it is clear that, after a transient regime, this will yield a zero value,* $L_{\text{yap}} = 0$, *for the Lyapunov*.

4.3. Phase portrait and Lyapunov characteristic exponents for $\epsilon = 0.185$*: the elliptic regions*

In order to compare the real Arnold complexity and the metric entropy (or in practice the Lyapunov characteristic exponents), let us consider the value[28] $\epsilon = 0.185$, which corresponds to a non-trivial real topological entropy ($\simeq \ln(1.38)$). This choice corresponds to a value of ϵ around which the real Arnold complexity has a rich enough

[28] We have performed similar calculations for many other values of ϵ yielding similar results.

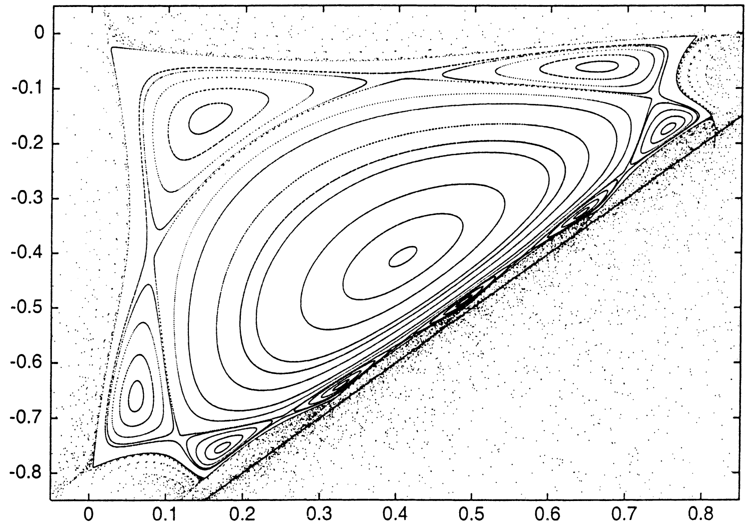

Fig. 4. Phase portrait for $\epsilon = 0.185$ in the (y, z) variables.

behavior (see Fig. 1), and such that one gets enough real fixed points of k_ϵ^N in a finite region of the (y, z)-plane, as can be seen in Fig. 4 which represents the phase portrait of the mapping in the (y, z) variables for $\epsilon = 0.185$.

The previously described program yields, for all the regular orbits (curves) in the elliptic regions, Lyapunov characteristic exponents equal to zero.

Fig. 5 gives $L_1^{(N)}$ and $L_2^{(N)}$, as a function of N, for a typical orbit in the main regular elliptic region of Fig. 4. Both values of $L_1^{(N)}$ and $L_2^{(N)}$ seem to decrease and to tend to zero, as a function of N, like some power law, as will be seen later. This zero limit can, heuristically, be understood in the same way as in the previously described integrable situation in elliptic regions, yielding, again, a zero value for the Lyapunov exponent, the only difference being that the integrable algebraic curves are replaced by transcendental curves, the movement on these transcendental curves being again a shift, $\theta \to \theta + \lambda$, in some well-suited variable θ. Do note that this kind of heuristic argument cannot

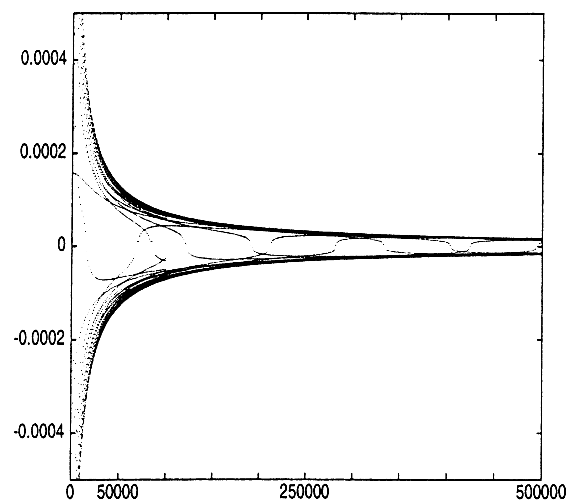

Fig. 5. $L_1^{(N)}$ and $L_2^{(N)}$, as a function of N, for an orbit in the elliptic region of Fig. 4.

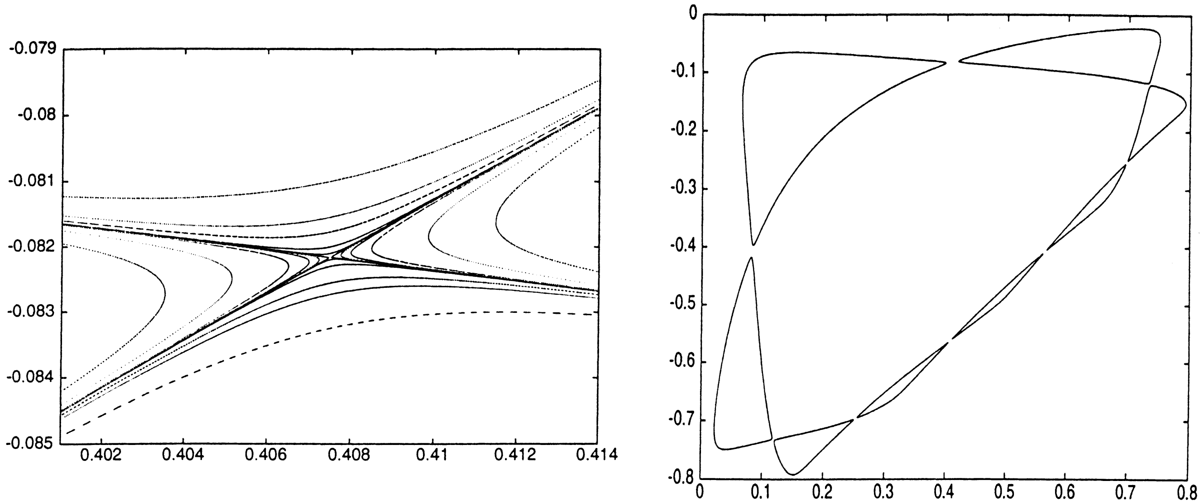

Fig. 6. Zoom of the phase portrait for $\epsilon = 0.185$ in the (y, z) variables near a hyperbolic point (left). One orbit sandwiched between the internal and external orbits (right).

be applied to a strange attractor (even if it is compact and even if it may look, for fractal dimension close to 1, similar to the previous curves). For a strange attractor a continuous variable like θ would not be well suited to describe the wandering of the point in the fractal structure. In fact, a continuous variable like θ does not exist for strange attractors. Two very close points will systematically see their mutual distance grow exponentially (finite positive Lyapunov) since they will wander in different parts of the fractal structure after a certain number of iterations.

4.4. *Phase portrait and Lyapunov characteristic exponent for $\epsilon = 0.185$: the hyperbolic points near the elliptic regions*

When one looks at the phase portrait of Fig. 4, one sees some bubble-like curves (see Fig. 6 (right)) sandwiched between two set of curves (see Fig. 7). This indicates the existence of hyperbolic points which balance the elliptic fixed points at the center of the previous bubbles. Let us first analyze such hyperbolic fixed points located near elliptic regions. Since Poincaré [72], the neighborhood of hyperbolic points [29] is known to be an appropriate locus for seeking for chaos. Fig. 6 shows that these hyperbolic points located near the elliptic regions are not of the chaotic type described by Poincaré [72] (infinite set of homoclinic points, intersections of the stable and unstable manifolds) but correspond to a nice foliation looking, locally, like hyperbole, as can be seen in Fig. 6 (left). Fig. 7 shows that this local hyperbola-like foliation is, in fact, part of global elliptic foliations. In the limit where the elliptic orbits get closer and closer to the hyperbolic points, one gets sharp pointed orbits near the hyperbolic points, like “corners” (see Fig. 7). There is no room left for the “Poincaré chaos” (see Fig. 6 (left)).

Fig. 6 (left) shows, in the (y, z) variables, the phase portrait for $\epsilon = 0.185$ near a hyperbolic point. Fig. 6 (left) is in perfect agreement with the calculated slope of the stable and unstable manifolds. In Fig. 6 (left), one can figure out that the stable and unstable manifolds are locally extremely regular having, locally, no intersection except at the very hyperbolic point. Fig. 6 (right) shows an orbit sandwiched between the internal and external orbit of Fig. 7. One sees that the orbit of Fig. 6 (right) is made of eight bubbles surrounding the elliptic fixed points of

[29] Poincaré [72] discovered that, for chaotic systems, the stable and unstable manifolds corresponding to the linearization around a hyperbolic fixed point intersect in an infinite set of homoclinic points [73]: this monstrous situation is the very expression of chaos.

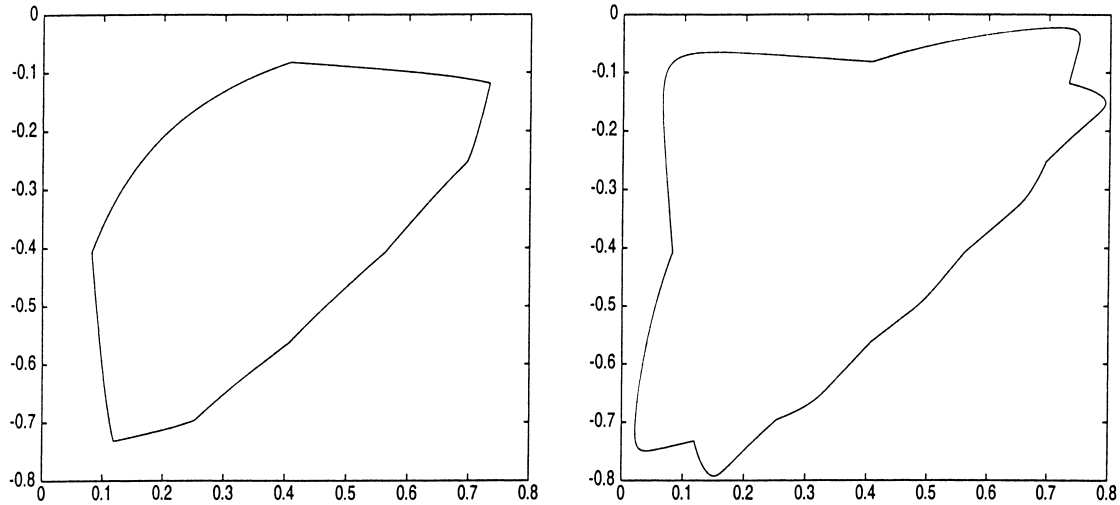

Fig. 7. One internal orbit of k_ϵ, for $\epsilon = 0.185$, getting very close to hyperbolic points (left). One external orbit of k_ϵ for $\epsilon = 0.185$ getting very close to the same hyperbolic points (right).

order eight. Actually, one also remarks that each bubble can be seen as an orbit of k_ϵ^8, and that k_ϵ^8 does not "mix" together these eight connected components. The orbits of Fig. 7 correspond to curves which combine together the stable and unstable manifolds described by Poincaré. Instead of being highly complicated twisted curves having an infinite number of (homoclinic points) intersections, they are extremely simple, and regular, with no intersections, even globally, far from the hyperbolic points. This extreme regularity near the hyperbolic points (see Fig. 6 (left)) excludes the Poincaré chaos.

Let us calculate the Lyapunov characteristic exponents for the previous three orbits: the internal, the external and the sandwiched bubble-like one. We represent here $L_1^{(N)}$ and $L_2^{(N)}$, as a function of N, the number of iterations.

Fig. 8 represents $L_1^{(N)}$ and $L_2^{(N)}$, as a function of N, the number of iterations for $\epsilon = 0.185$ and for the external orbit of Fig. 7 (right). However, one must remark that one obtains almost indistinguishable plots for the internal orbit of Fig. 7 (left), as well as for the sandwiched orbit of Fig. 6 (right). One also sees, beyond doubt, that the limits

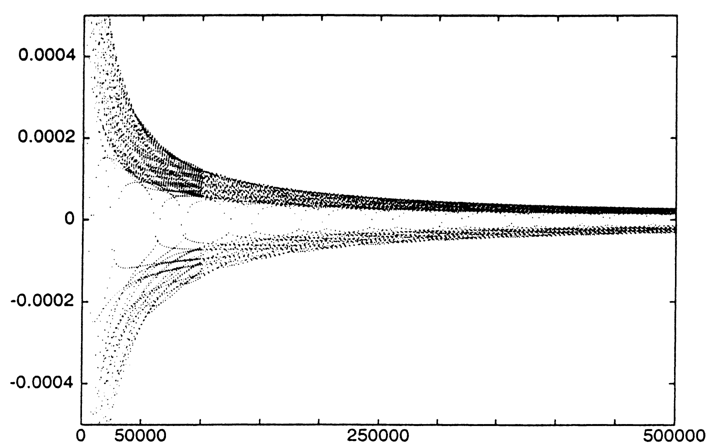

Fig. 8. $L_1^{(N)}$ and $L_2^{(N)}$, as a function of N, the number of iterations for $\epsilon = 0.185$ for the external orbit of Fig. 7.

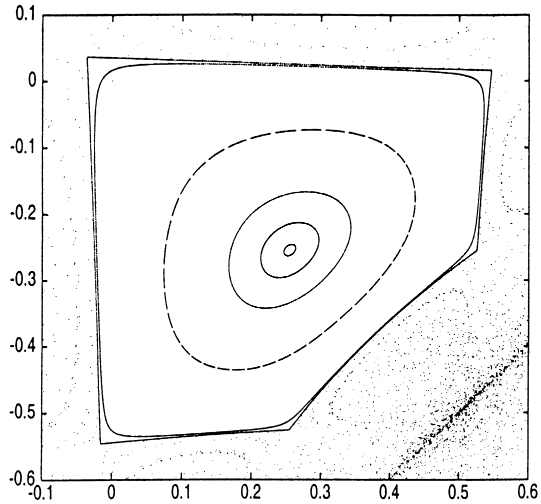

Fig. 9. A phase portrait to visualize the frontier between the regular elliptic region and the spray-like region for $\epsilon = 0.49$.

of $L_1^{(N)}$ and $L_2^{(N)}$, go to zero and, therefore, that the Lyapunov characteristic exponents should be equal to zero, for these curves, globally elliptic with their eight hyperbolic corners.

4.5. Phase portrait and Lyapunov characteristic exponent for $\epsilon = 0.185$: the hyperbolic points near the "spray-like" region

Since one heuristically understands that Lyapunov characteristic exponents should be equal to zero in the elliptic regions, even for orbits passing near hyperbolic points, one can only expect that a more spray-like region, like the one which can be seen in Fig. 4, is where chaos could possibly occur, yielding (at least!) non-zero Lyapunov exponents.

Let us consider an elliptic orbit which could "mimic" the frontier between the elliptic region in Fig. 4 and a more spray-like region where chaos seems to occur, possibly yielding non-zero Lyapunov exponents. Let us change here the value of ϵ in order to have a simpler diamond-shaped frontier than the frontier, one can imagine from Fig. 4. For this, we consider, in this section, a value [30] of ϵ near the integrable value $\epsilon = \frac{1}{2}$, namely $\epsilon = 0.49$.

Again, let us calculate the Lyapunov characteristic exponent for an orbit in the elliptic region, but near the frontier, and let us compare it with the Lyapunov characteristic exponent for an orbit in the spray-like region corresponding to an initial point near this frontier (see Fig. 9).

One sees, quite clearly in Fig. 10 that the Lyapunov characteristic exponent, for the orbit in the elliptic region (corresponding to (I) in Fig. 10) seems to be equal to zero, and this also seems to be the case for the orbit near the diamond-shaped frontier, in the spray-like region (corresponding to (II) in Fig. 10). Fig. 10 (right) is a magnification of $L_1^{(N)}$ and $L_2^{(N)}$, as a function of N, for the first 1×10^4 iterations. In fact, we have performed a large number of Lyapunov calculations for various orbits outside the elliptic region, in this spray-like region which seems to be controlled by the point at infinity (see also Section 4.6). All these Lyapunov calculations seem to indicate (after 5×10^5 iterations) that one has a Lyapunov characteristic exponent equal to zero, namely $L_i^{(N)} \to 0 \ \ (i = 1, 2)$. A

[30] One gets similar results for the previous $\epsilon = 0.185$ value.

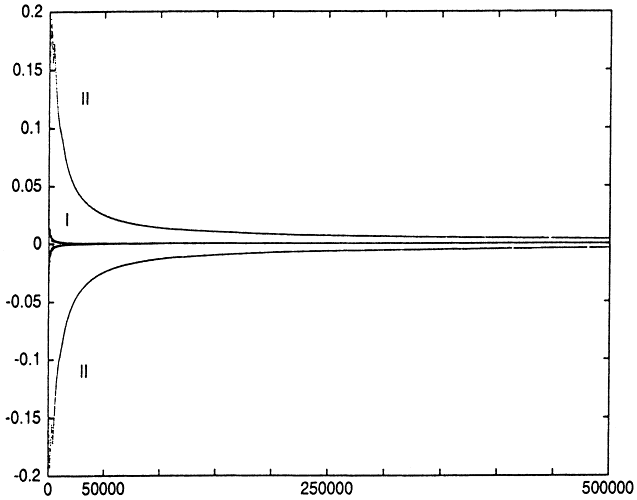

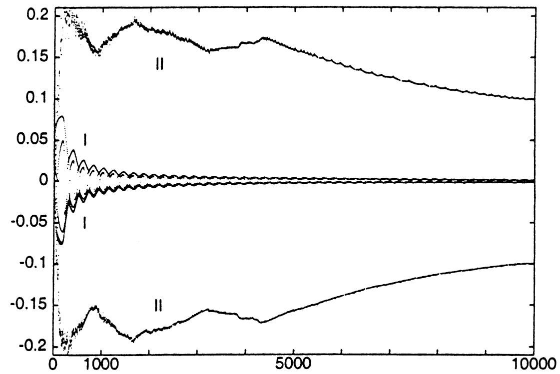

Fig. 10. $L_1^{(N)}$ and $L_2^{(N)}$, as a function of N, for $\epsilon = 0.49$, for an orbit in the elliptic region but near the frontier, indexed by (I), and for an orbit, indexed by (II), in the spray-like region, corresponding to an initial point near this frontier. These $L_i^{(N)}$'s are given for 5×10^5 iterations (left) and for only 1×10^4 iterations (right).

more precise analysis shows that the $L_i^{(N)}$'s seem, phenomenologically, to behave like

$$L_i^{(N)} = \frac{\ln(|\lambda_i^{(N)}|)}{N} \simeq N^{\alpha}, \quad i = 1, 2, \tag{40}$$

where the exponent α seems to be the same for $L_1^{(N)}$ and $L_2^{(N)}$. More details are given in Appendix B. Appendix B underlines that the extensivity of the $\ln(|\lambda_i^{(N)}|)$'s is certainly not satisfied: one has here an under-extensive behavior for the $\ln(|\lambda_i^{(N)}|)$'s yielding Lyapunov exponents equal to zero.

4.6. Lyapunov characteristic exponents in the spray-like region near the point at infinity

Let us now try to calculate, again, Lyapunov characteristic exponents for other orbits (that will be depicted in the next sections), in the spray-like region dominated by the point at infinity. These orbits yield systematically the $L_i^{(N)}$'s to tend to zero, as a function of N, and one can see, again, that the $\ln(|\lambda_i^{(N)}|)$'s are certainly not extensive quantities such that the limit of the $L_i^{(N)}$'s could be a non-zero finite value when N gets large.

Fig. 11 represents the $L_i^{(N)}$'s, as a function of N, for four orbits (like Fig. 15) corresponding to four initial points near the point at infinity $(Y, Z) = (0, 0)$. These four orbits correspond to the iteration of an initial point $(Y, Z) = (-3\delta, 4\delta)$ for four different values of δ, namely $\delta = 1 \times 10^{-5}$, 1×10^{-3}, 1×10^{-2} and 1×10^{-1}. For an initial point very close to $(Y, Z) = (0, 0)$ (namely $\delta = 1 \times 10^{-5}$, curve (1) in Fig. 11), the $L_i^{(N)}$'s take very small values ($\simeq 1 \times 10^{-5}$), and seem to have a zero limit when N gets large. The zero limit for the $L_i^{(N)}$'s, when N gets large, is also very clear for the two other initial points corresponding, respectively, to $\delta = 1 \times 10^{-3}$ and 1×10^{-2} (curves (2) and (3) in Fig. 11). The last initial point yields a less obvious zero limit for the $L_i^{(N)}$'s, however, one can see that the local deviation around 2.5×10^5 iterations is similar to other deviations one can see for other orbits which actually yield, for N large enough, a zero limit for the $L_i^{(N)}$'s. Let us also remark that this local deviation of the $L_i^{(N)}$'s around 2.5×10^5 iterations does not correspond to the orbit exploring some new domain of the phase space (like getting trapped in some strange attractor, etc.). The orbit, before 2.5×10^5 iterations, and after 2.5×10^5

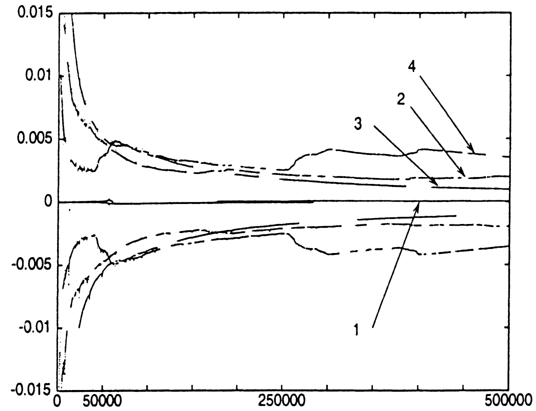

Fig. 11. The $L_i^{(N)}$'s, as a function of N, corresponding to four orbits of an initial point $(Y, Z) = (-3\delta, 4\delta)$ near the point at infinity $(Y, Z) = (0, 0)$. Curves (1), (2), (3) and (4) correspond to $\delta = 1 \times 10^{-5}$, 1×10^{-3}, 1×10^{-2} and 1×10^{-1}, respectively.

iterations, are really on the same footing. In addition to the global $L_i^{(N)} \to 0$ trend, one just sees some modulation phenomenon for $L_i^{(N)}$, as a function of N. These modulations will be studied elsewhere.

To sum up, all our calculations yield a non-extensive behavior for the $L_i^{(N)}$'s, as a function of N, for orbits inside the spray-like region, suggesting zero Lyapunov characteristic exponents. They thus seem to show that the *metric entropy is either equal to zero* or, in any case, *significantly smaller than the topological entropy and, even, the real topological entropy*.

Remark (Lyapunov characteristic exponents of complex orbits). *As far as Lyapunov's calculations with our infinite precision program are concerned, one can modify the program in order to calculate the $L_i^{(N)}$'s for orbits corresponding to the iterations of a complex initial point (y, z) instead of a* real *one. All the calculations performed give similar results: the Lyapunov characteristic exponents, or at least the $L_i^{(N)}$'s, were not significantly larger, for complex orbits,*[31] *as compared to the ones for real orbits. Of course, since the set of initial complex points is much larger compared to the set of initial real points, we cannot claim that the Lyapunov characteristic exponents of all the complex orbits are equal to zero or are very small.*

5. Heuristic interpretation of the zero Lyapunov in the spray-like region

The analysis of the previous sections seems to show that the $L_i^{(N)}$'s tend to zero, as a function of N, even in the spray-like region, for which the orbit is not confined to any elliptic regular region, and for which one could have expected some chaos. The only difference with the elliptic regular regions is that the convergence to zero is slower. Let us try to understand this numerical result.

For the orbits in the spray-like region, the points seem to wander in the plane, getting quite far from the main elliptic region towards the point at infinity, then coming back towards the elliptic region and again getting far towards the point at infinity, and again — balancing indefinitely between these two regions. In order to better understand this situation, let us consider the neighborhood of the point at infinity by performing a change of variables. For this, let us change (y, z) into $(Y, Z) = (1/y, 1/z)$. Then mapping (1) becomes

[31] The Lyapunov exponents of complex orbits of polynomial diffeomorphisms are discussed in [74].

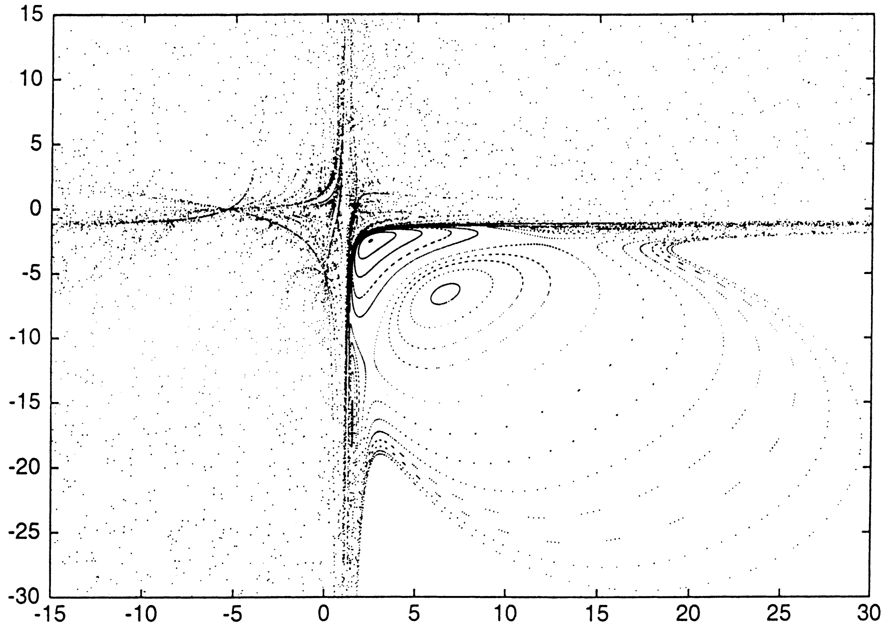

Fig. 12. Phase portrait for $\epsilon = 0.185$ in the (Y, Z) variables.

$$k_\epsilon : (Y, Z) \to \left(\frac{Z}{1 + (1-\epsilon)Z}, Y \frac{1+Z}{1-\epsilon Z} \right). \tag{41}$$

One can now revisit the phase portrait of Fig. 4 in these new (Y, Z) variables, well suited to analyze the vicinity of the point at infinity, which is another fixed point of the mapping (see Fig. 12).

5.1. Analysis near the point at infinity: seeking for transcendental invariants

Zooming the previous phase portrait, near the point at infinity $(Y, Z) = (0, 0)$, one gets a surprisingly regular phase portrait. The points seem to form a very regular foliation.

Fig. 13 indicates a phase portrait corresponding very much to a foliation (at least for (Y, Z) small enough) and shows, furthermore, a remarkable structural instability. [32] To see this, let us plot the first 10 000 iterations of a single orbit of a point near the point at infinity $(Y, Z) = (0, 0)$.

One can (at least near the point at infinity $(Y, Z) = (0, 0)$) imagine an interpretation of the orbit as a transcendental curve, made of an infinite number of branches, each branch looking very much like a curve. If one goes on iterating k_ϵ and not k_ϵ^{-1}, one gets more and more branches going, each time, closer and closer to the point at infinity $(Y, Z) = (0, 0)$. This transcendental curve has an infinite number of branches (the price to pay for being transcendent, etc.). Fig. 14 illustrates this interpretation giving the first branches of this infinite set of branches.

Near the fixed point at infinity, $(Y, Z) = (0, 0)$, the phase portrait looks very much like a hyperbola-like foliation but with three asymptotes instead of two. A first approximation of the equations of these branches could be $YZ(Y - Z) \simeq \rho$, where ρ is a constant. Considering a simple linearization around the $(Y, Z) = (0, 0)$ fixed point, it

[32] The notion of structural stability has been introduced by Andronov and Pontryaguin [75]. A structurally stable [75,76] dynamical system is a system such that its phase portrait is slightly modified, and remains topologically similar, under small perturbations of the system. Most of the two-dimensional dynamical systems are structurally stable, this is no longer the case in dimensions greater than 2.

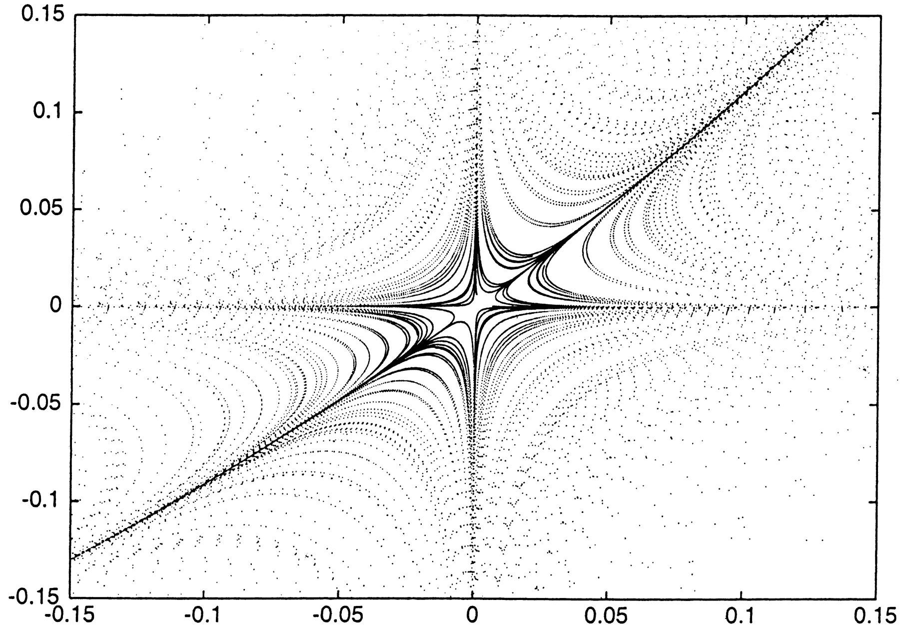

Fig. 13. Phase portrait for $\epsilon = 0.185$ in the (Y, Z) variables near the point at infinity $(Y, Z) = (0, 0)$.

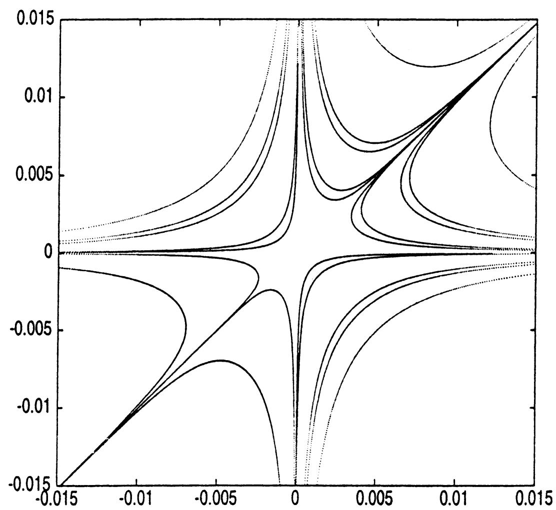

Fig. 14. A single orbit of a point near the point at infinity $(Y, Z) = (0, 0)$ for $\epsilon = 0.185$.

seems, at first sight, difficult to understand these three singled-out directions (three eigenvectors of the 2×2 matrix corresponding to the linearized part of transformation (41), etc.). In fact, this structural instability can be understood as follows: the linearization of the square [33] of transformation (41) around $(Y, Z) = (0, 0)$ gives (at order three)

[33] If, instead of the square of transformation (41), one linearizes transformation (41) itself, one gets a transformation which gives at the first-order $(Y, Z) \to (Z, Y) + \cdots$.

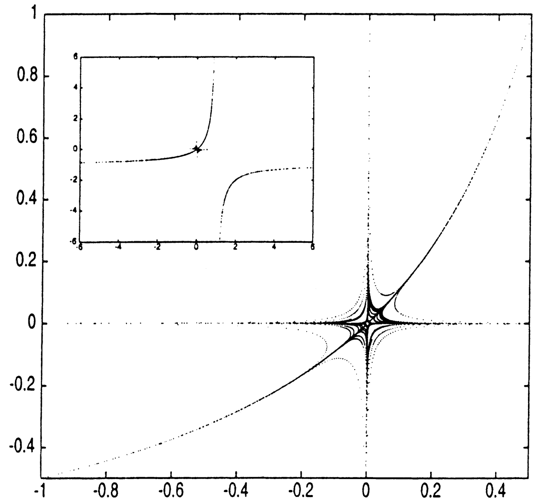

Fig. 15. The single orbit of Fig. 14 with a larger scale.

$$Y \to Y_1 = Y + Y((\epsilon - 1)Y + (1+\epsilon)Z) + Y(-2YZ + \epsilon Z^2 + \epsilon^2 Z^2 + 2\epsilon^2 YZ + Y^2 - 2\epsilon Y^2 + \epsilon^2 Y^2) + \cdots,$$
$$Z \to Z_1 = Z + Z((\epsilon - 1)Z + (1+\epsilon)Y) + Z(2\epsilon YZ + \epsilon Y^2 + 2\epsilon^2 YZ + \epsilon^2 Y^2 - 2\epsilon Z^2 + \epsilon^2 Z^2 + Z^2) + \cdots. \quad (42)$$

We are thus in the situation of a diffeomorphism tangent to identity (see also [77]), thus allowing, around the fixed point at infinity $(Y, Z) = (0, 0)$, the appearance of three singled-out directions, instead of the generic two eigenvectors for linearized two-dimensional mappings (tangent map).

In fact $Y - Z = 0$ is the first-order approximation for one of the three asymptotes, as can be seen, easily, in Fig. 14. However, one can see, that this is just the first-order approximation of a slightly more complicated algebraic expression, namely $(1-Y)(1+Z)-1=0$, as can be seen by looking at the orbit of Fig. 14, but with a larger scale. The hyperbola $(1-Y)(1+Z)-1=0$ corresponds to the singled-out globally invariant line $y = 1+z$ written in terms of the (Y, Z) variables. This is quite clear in Fig. 15, and in particular, on the insert, in Fig. 15.

Therefore, a second approximation for the transcendental invariant could be

$$\mathcal{I}_1 = YZ(1-(1-Y)(1+Z)) + \cdots = YZ(Y - Z + YZ) + \cdots. \quad (43)$$

Actually $\mathcal{I}_1 = \rho$ is a quite good approximation of the various branches one sees in Figs. 13 and 14 or in Fig. 15. This gives some hope of a possible heuristic description of the movement on these transcendental curves as a shift $t \to t + \rho$ in some well-suited variables, again yielding zero Lyapunov exponents. Of course, all these calculations should only be considered as a very preliminary heuristic description of this diffeomorphism tangent to identity (see also [77]). Let us make a few comments on the fact that Fig. 13 looks like a foliation. In Fig. 14, one seems to get (at least near the point at infinity, etc.) curves, however, the way these curves are densified is slow as compared to the previously described way transcendental curves are densified in the elliptic regions (a situation isomorphic to a rotation on a unit circle). The way these curves are densified is more like a shift on the real axis ($t \to t + \rho$), i.e. a "borderline" parabolic situation between the elliptic situation ($\theta \to \theta + \lambda$) and the hyperbolic situation ($x \to \mu x$). This fact will be fully confirmed later by the analysis of the $\epsilon = 3$ case (see Section 6) which gives some idea of what a transcendental curve could be. Looking at the infinite number of branches of an orbit when one moves away from the point at infinity (see Fig. 13), one can imagine that the set of points could actually be on curves, but that

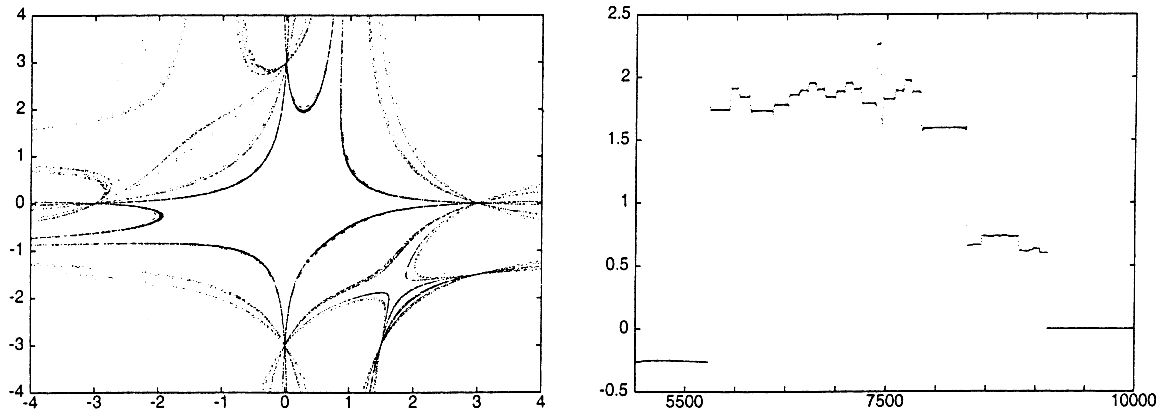

Fig. 16. Left: A single orbit in the (Y, Z) variables for $\epsilon = 0.33333$ corresponding to the deformation of the $\epsilon = \frac{1}{3}$ integrable algebraic foliation (45). Right: $I_{\mathrm{nv}}(\epsilon = \frac{1}{3})$ as a function of the number of iterations for the previous orbit.

the "lazy" way of densifying the curves ($t \to t + \rho$) gives, more and more, the feeling of a spray of points. This spray point of view is the one that dominates at the scale of Fig. 12.

One may consider that the question of qualifying transcendental curve, the single orbit of Fig. 14 is a quite metaphysical question. Therefore, let us give, in Section 5.2, another heuristic interpretation that does not rely on such a transcendental curve notion, but also tries to explain the vanishing of the Lyapunov characteristic exponents.

5.2. *An alternative interpretation: deformation of the algebraic foliation for $\epsilon \simeq \frac{1}{3}$*

One verifies, quite easily using (42), that the square of transformation (41) acting on (43) yields, at order four in Y and Z that

$$(\mathcal{I}_1, \mathcal{I}_2) \to (\mathcal{I}_1 + \mathcal{I}_2, \mathcal{I}_2) + \cdots , \tag{44}$$

where $\mathcal{I}_2 = (3\epsilon - 1)(Y + Z)\mathcal{I}_1 + \cdots$. These calculations seem to suggest a perturbative approach near the $\epsilon = \frac{1}{3}$ integrable value. In this respect, let us recall the invariant for the integrable $\epsilon = \frac{1}{3}$ situation written in the (Y, Z) variables. It reads [37] that

$$I_{\mathrm{nv}}(\epsilon = \tfrac{1}{3}) = \frac{Y^2 Z^2 (YZ + Y - Z)^2}{(3 + Y + Z + YZ)(3 - Y + Z - YZ)(3 - Y - Z + YZ)(9 + 3Y - 3Z + 5YZ)}. \tag{45}$$

In Fig. 16, one sees, quite clearly, how a single orbit for $\epsilon = 0.33333$ can be seen to be related to the elliptic foliation for $\epsilon = \frac{1}{3}$.

In particular, one sees that the base points of the algebraic foliation (45) do play a singled-out role for the orbit of Fig. 16. This special role is confirmed by Fig. 17 which shows a single orbit associated with a larger deformation from $\epsilon = \frac{1}{3}$, namely $\epsilon = 0.3333$.

In Fig. 17, one recovers a situation very similar to the one depicted in Fig. 13, namely some branches which look very much like curves and other branches which are probably curves also, but densified in a more "sparse" way. A single orbit, like Fig. 16 or Fig. 17 (left), is heuristically, in a first approximation, like a set of curves of the algebraic foliation (45), the successive values of $I_{\mathrm{nv}}(\epsilon = \frac{1}{3})$ one encounters being described by the step-like functions of Fig. 16 or Fig. 17 (right). The transition, from one value of $I_{\mathrm{nv}}(\epsilon = \frac{1}{3})$ to another one, occurs near the base points of foliation (45) (as one could have easily guessed). Note that considering the inverse transformation k_ϵ^{-1}, the same

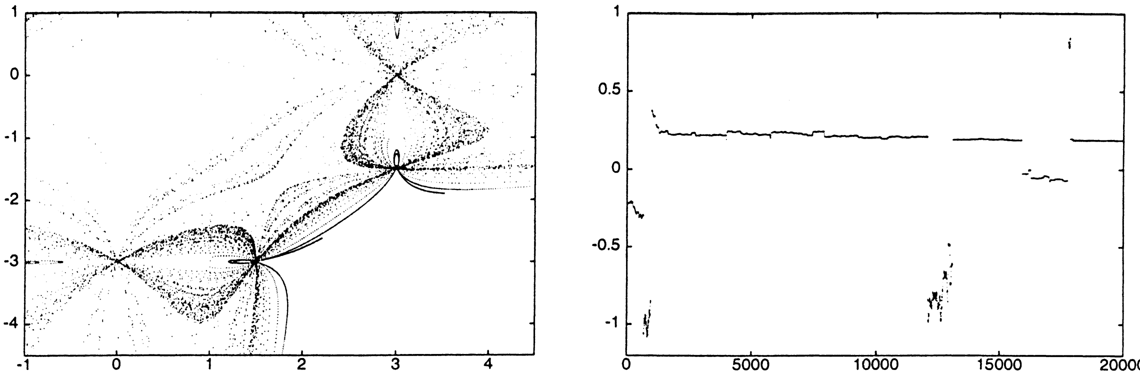

Fig. 17. Left: One orbit for $\epsilon = 0.3333$ corresponding to the deformation of the $\epsilon = \frac{1}{3}$ integrable algebraic foliation. Right: $I_{\rm nv}(\epsilon = \frac{1}{3})$ as a function of the number of iterations for the previous orbit.

set of values of $I_{\rm nv}(\epsilon = \frac{1}{3})$ will be encountered successively, but in the reversed order. All these calculations have been performed with our infinite precision gmp program: all the points, and all the values of $I_{\rm nv}(\epsilon = \frac{1}{3})$, are exact, there is no numerical deviations.

This heuristic interpretation of the orbit as an exploration of successive values of $I_{\rm nv}(\epsilon = \frac{1}{3})$ is still, to a large extent, valid for a larger deformation from $\epsilon = \frac{1}{3}$ like the one of Fig. 18 which corresponds to $\epsilon = 0.333$, with the only difference that the lengths of some intervals of the step-like functions depicted in Fig. 18 (right) become, sometimes, quite small. The orbit description presented here does not require a concept like the notion of transcendental curve. It corresponds to a weaker kind of compatibility of the true orbit with curves, namely some "hopping" in a set of curves. In this approximation, the previous $\theta \to \theta + \lambda$ shift argument yielding zero Lyapunov exponents is certainly valid when one moves on each of these curves corresponding to these particular values of $I_{\rm nv}(\epsilon = \frac{1}{3})$, and thus, on the whole orbit. The various right figures of Figs. 16–18 correspond to a quite good approximation of these orbits (whatever they actually are, etc.) as a successive exploration of various curves of the integrable algebraic foliation (45). This heuristic description of the orbits is in agreement with the zero value of the Lyapunov characteristic exponent encountered in the three previous cases (and in many others).

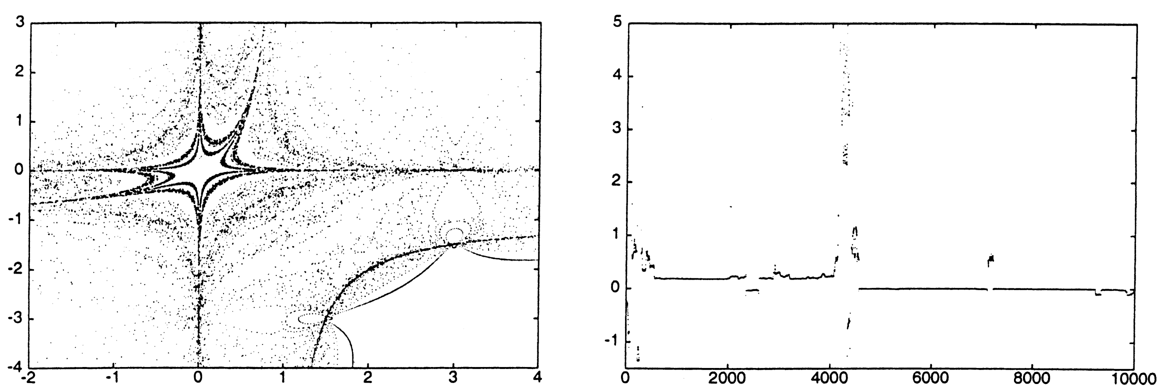

Fig. 18. Left: One orbit for $\epsilon = 0.333$ corresponding to the deformation of the $\epsilon = \frac{1}{3}$ integrable algebraic foliation. Right: $I_{\rm nv}(\epsilon = \frac{1}{3})$ as a function of the number of iterations for the previous orbit.

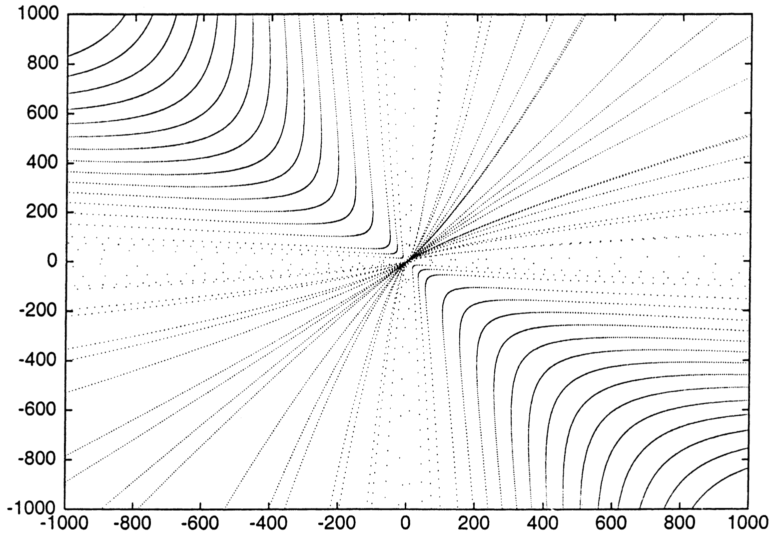

Fig. 19. Phase portrait in the (y, z) variables of the birational transformation (1), for $\epsilon = 3$, near the fixed point of k_ϵ.

Remark. *All the previous computations of Lyapunov exponents at various points representative of the phase space, come up with exponents equal to* 0, *or, at least, very small. However, since the topological entropy is positive* (*even the real topological entropy, except around* $\epsilon \simeq 3$), *there must exist some invariant measure with positive entropy. The important question would be to find out typical points with respect to this invariant measure and find their positive Lyapunov exponents. Beyond a quite systematic analysis of real* (y, z) *points, all our infinite precision computer calculations have failed to localize such typical points.* (*Are they complex points localized near the* $y = 1 + z$ *line, or near the indeterminacy locus*?)

6. The birational transformation (41) for $\epsilon = 3$

As far as a comparison between the metric entropy and the real topological entropy, or the real Arnold complexity, is concerned, $\epsilon = 3$ is obviously an interesting singled-out value, for which one can claim that the real topological entropy is, not only extremely small, but really equal to zero (see (23) and also (28)). Therefore, one can expect, for this very value, a very clean comparison between the metric entropy and the real topological entropy, or the real Arnold complexity.

Let us thus consider the birational transformation (1) for $\epsilon = 3$. This value of ϵ is singled out as far as the phase portrait of transformation (1) is concerned: instead of a quite chaotic phase portrait in the (y, z) variables (see Fig. 3 in [33]), the iteration of k_ϵ for $\epsilon = 3$ gives a very regular phase portrait in the (y, z)-plane, especially around the fixed point of k_ϵ for $\epsilon = 3$: $(y, z) = (-1, 1)$. Fig. 19 seems to indicates a structural instability [75] of a slightly different nature than the one which pops out in Figs. 13 and 14 above. Instead of having hyperbola-like curves with three asymptotes, one sees, at the scale of Fig. 19 and in the (y, z) variables, three singled-out directions. In fact, a magnification of the neighborhood of the fixed point obviously shows a structural instability (see Figs. 19 and 20).

In order to get some simple hint on this new structural instability [75], let us linearize transformation k_ϵ (see (1)) near its fixed point. For generic values of ϵ, the linearization of (1) near the fixed point of k_ϵ^3, $(y, z) = (-1, 1)$, gives, with the notations $y = -1 + \delta_y,\ z = 1 + \delta_z$:

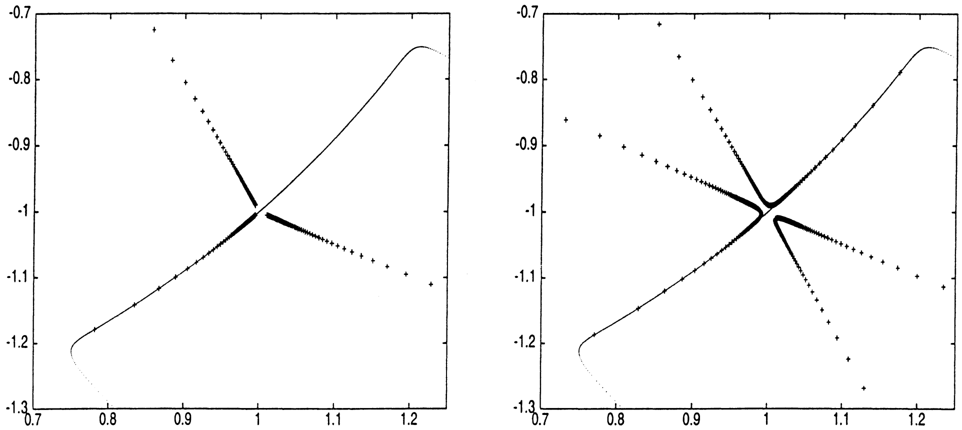

Fig. 20. Left: A single orbit of (1) corresponding to 2000 iterations of an initial point $(y, z) = (1 + \epsilon_1, -1 + \epsilon_1)$ very near the fixed point of (1). The curve corresponds to the polynomial of degree 36 associated with the truncation of the divergent series (56). Right: A single orbit of an initial point $(y, z) = (1 + \epsilon_1, -1 + \epsilon_1)$ slightly further the fixed point of (1).

$$\delta_y \to 2\frac{(\epsilon-1)(-2+\epsilon)}{\epsilon+1}\delta_y + (\epsilon-3)\delta_z + \cdots , \qquad \delta_z \to (3-\epsilon)\delta_y - \frac{(\epsilon+1)(\epsilon-4)}{2(\epsilon-1)}\delta_z + \cdots , \tag{46}$$

where the Jacobian matrix of this tangent map has a determinant equal to 1. In the $\epsilon \to 3$ limit, relation (46) becomes at the first order: $(\delta_y, \delta_z) \to (\delta_y, \delta_z)$. One has, again, a diffeomorphism tangent to identity. This very fact allows the existence of three singled-out directions (see Fig. 20).

6.1. An exact functional equation for $\epsilon = 3$

The orbits for $\epsilon = 3$ (see Fig. 19) seem to be curves, exactly similar to the foliation of the plane in algebraic elliptic curves (linear pencil of elliptic curves) one gets for integrable mappings [32], although the $\epsilon = 3$ value can actually be seen to correspond [35] to the chaotic complexity $\lambda \simeq 1.61803$ (generic complexity value, see (14)). The question we address in this section is how to reconcile these apparently opposite facts. For this, let us first introduce a parameterization of these curves: $(y, z) = (y(t), z(t))$, and let us consider the representation, restricted to these curves, of k_ϵ in terms of this parameter t.

In fact, a visualization of the curves obtained by the iteration of k_ϵ for $\epsilon = 3$, singles out three curves, Γ_1, Γ_2 and Γ_3, intersecting at the fixed point of k_ϵ for $\epsilon = 3$, namely $(y, z) = (-1, 1)$, which play, more or less, the role of the stable and instable manifolds, but there are three of them! Note that each curve is globally stable by k_ϵ^3, and that k_ϵ, and k_ϵ^2, map one of the three curves Γ_i into the two others. The appearance of these three curves Γ_i is reminiscent of the coalescence, in the $\epsilon \to 3$, limit of the three fixed points of k_ϵ^3, namely $(y, z) = (2-\epsilon, \frac{1}{2}(\epsilon-1))$ or $(\frac{1}{2}(1-\epsilon), \epsilon-2)$ or $(-1, 1)$, with the fixed point of k_ϵ, namely $(\frac{1}{2}(1-\epsilon), \frac{1}{2}(\epsilon-1))$. In this limit, the triangle, made from these three confluent fixed points, actually corresponds to the three directions, at $(y, z) = (-1, 1)$, of the three singled-out curves Γ_i (see below).

Let us concentrate on one of these three curves, Γ_1. Since Γ_1 is globally stable by k_ϵ^3 but not by k_ϵ, one can only expect a representation of k_ϵ^3 (and not of k_ϵ) in terms of a well-suited variable t around the fixed point of k_ϵ: $(y, z) = (-1, 1)$. Recalling transformation (1), yields, for $\epsilon = 3$, the following expressions for the two y and z components of k_ϵ^3:

$$k_y^3 = \frac{4+12y+z-7yz-3z^2+yz^2}{1-3y+z+yz}, \qquad k_z^3 = \frac{(yz-2-3y-2z)(3+15y-8yz-3z^2+yz^2)}{(7+3y+4z-4yz-3z^2+yz^2)(1+z)}. \tag{47}$$

Let us now try to find the parameterization $(y(t), z(t))$ of curves Γ_i (as an expansion near the fixed point of k_ϵ for $\epsilon = 3$, namely $(y, z) = (-1, 1)$ which belongs to the curves). A simple linearization of k_ϵ^3 around this fixed point $(y, z) = (-1, 1)$ yields the identity matrix: therefore, one cannot have (near this fixed point) a representation of the iteration of k_ϵ^3 like $t \to \mu t$, it must be a shift representation $t \to \mu + t$. However, such a shift representation is not well suited to deal with an expansion around the fixed point $(y, z) = (-1, 1)$ (the fixed point would correspond to $t = \infty$). We must represent the shift, associated with the action of k_ϵ, as $t \to t/(1+t)$, i.e. $1/t \to 1/(t+1)$. Let us then write, using this last shift representation, that one of the (three) curves, namely Γ_1, is actually invariant under k_ϵ^3:

$$k_y^3(t) = y\left(\frac{t}{1+t}\right), \qquad k_z^3(t) = z\left(\frac{t}{1+t}\right). \tag{48}$$

Eq. (48), when solved, gives, order by order, three solutions. One solution corresponds to the following expansion, depending on only one parameter σ, for $y(t)$ and $z(t)$:

$$\begin{aligned} y(\sigma, t) = {} & -1 + \frac{2}{3}t - \sigma t^2 - \left(\frac{10}{81} - \frac{3}{2}\sigma^2\right) t^3 + \left(\frac{5}{729} + \frac{5}{9}\sigma - \frac{9}{4}\sigma^3\right) t^4 \\ & + \left(\frac{545}{6561} - \frac{10}{243}\sigma - \frac{5}{3}\sigma^2 + \frac{27}{8}\sigma^4\right) t^5 - \left(\frac{1085}{78732} + \frac{2725}{4374}\sigma - \frac{25}{162}\sigma^2 - \frac{25}{6}\sigma^3 + \frac{81}{16}\sigma^5\right) t^6 \\ & - \left(\frac{117935}{1062882} - \frac{1085}{8748}\sigma - \frac{2725}{972}\sigma^2 + \frac{25}{54}\sigma^3 + \frac{75}{8}\sigma^4 - \frac{243}{32}\sigma^6\right) t^7 \\ & + \left(\frac{73175}{2125764} + \frac{825545}{708588}\sigma - \frac{7595}{11664}\sigma^2 - \frac{19075}{1944}\sigma^3 + \frac{175}{144}\sigma^4 + \frac{315}{16}\sigma^5 - \frac{729}{64}\sigma^7\right) t^8 + \cdots, \end{aligned} \tag{49}$$

$$\begin{aligned} z(\sigma, t) = {} & 1 + \frac{2}{3}t - \left(\frac{4}{9} + \sigma\right) t^2 - \left(\frac{14}{81} - \frac{4}{3}\sigma - \frac{3}{2}\sigma^2\right) t^3 \\ & + \left(\frac{31}{729} - \frac{7}{9}\sigma - 3\sigma^2 - \frac{9}{4}\sigma^3\right) t^4 - \left(\frac{631}{6561} + \frac{62}{243}\sigma - \frac{7}{3}\sigma^2 - 6\sigma^3 - \frac{27}{8}\sigma^4\right) t^5 \\ & - \left(\frac{409}{26244} - \frac{3155}{4374}\sigma - \frac{155}{162}\sigma^2 + \frac{35}{6}\sigma^3 + \frac{45}{4}\sigma^4 + \frac{81}{16}\sigma^5\right) t^6 \\ & + \left(\frac{128683}{1062882} + \frac{409}{2916}\sigma - \frac{3155}{972}\sigma^2 - \frac{155}{54}\sigma^3 + \frac{105}{8}\sigma^4 + \frac{81}{4}\sigma^5 + \frac{243}{32}\sigma^6\right) t^7 \\ & + \left(\frac{35363}{6377292} - \frac{900781}{708588}\sigma - \frac{2863}{3888}\sigma^2 + \frac{22085}{1944}\sigma^3 + \frac{1085}{144}\sigma^4 \right. \\ & \left. - \frac{441}{16}\sigma^5 - \frac{567}{16}\sigma^6 - \frac{729}{64}\sigma^7\right) t^8 + \cdots. \end{aligned} \tag{50}$$

One thus gets (at first sight) a family of curves depending on one parameter, namely σ. In fact, this is not a family of curves: parameter σ corresponds to a simple reparameterization of a single curve. Considering expansions (49) and (50), one immediately verifies that

$$y(\sigma + \tfrac{2}{3}\tau, t) = y\left(\sigma, \frac{t}{(1+\tau t)}\right), \qquad z(\sigma + \tfrac{2}{3}\tau, t) = z\left(\sigma, \frac{t}{(1+\tau t)}\right). \tag{51}$$

This parameter σ corresponds to transformation $t \to t/(1+\tau t)$, which just amounts to changing the shift corresponding to k_ϵ^3, from (a normalized value) 1 to another value τ:

$$\frac{1}{t} \to \frac{1}{t} + \tau. \tag{52}$$

This means that one does not have a family of curves indexed by σ, but rather, a single curve with a reparameterization parameter σ. Therefore, without any loss of generality, one can restrict to a specific value of σ, for instance $\sigma = -\frac{2}{9}$. One then gets

$$y(t) = -1 + \frac{2}{3}t + \frac{2}{9}t^2 - \frac{4}{81}t^3 - \frac{67}{729}t^4 + \frac{119}{6561}t^5 + \frac{7031}{78732}t^6 - \frac{9004}{531441}t^7 - \frac{498563}{3188646}t^8 + \cdots, \tag{53}$$

$$z(t) = 1 + \frac{2}{3}t - \frac{2}{9}t^2 - \frac{4}{81}t^3 + \frac{67}{729}t^4 + \frac{119}{6561}t^5 - \frac{7031}{78732}t^6 - \frac{9004}{531441}t^7 + \frac{498563}{3188646}t^8 + \cdots. \tag{54}$$

One remarks, for this particular value $\sigma = -\frac{2}{9}$, the following relation:

$$y(t) = -z(-t). \tag{55}$$

This is a remarkable result: it means that, in order to get, order by order, the parameterization of the curve, one just needs to find the expansion of a only one function $y(t)$ instead of two ($y(t)$ and $z(t)$). The expansion of $y(t)$ at higher orders can be found in Appendix C. This divergent series seems to be Borel summable [78] (see also (69) in Appendix C).

This solution, corresponds to one of the three previously mentioned curves, say, Γ_1. The two other solutions of (48) correspond to the following expansions for $y(t)$ and $z(t)$, depending on a only one parameter, σ_2 or σ_3:

$$\begin{aligned} y(\sigma_2, t) &= -1 + \frac{2}{3}t - \sigma_2 t^2 - \left(\frac{10}{81} - \frac{3}{2}\sigma_2^2\right)t^3 - \left(\frac{5}{729} - \frac{5}{9}\sigma_2 + \frac{9}{4}\sigma_2^3\right)t^4 + \cdots, \\ z(\sigma_2, t) &= 1 - \frac{4}{3}t + \left(\frac{2}{9} + 2\sigma_2\right)t^2 + \left(\frac{2}{81} - \frac{2}{3}\sigma_2 - 3\sigma_2^2\right)t^3 - \left(\frac{2}{81} + \frac{1}{9}\sigma_2 - \frac{3}{2}\sigma_2^2 - \frac{9}{2}\sigma_2^3\right)t^4 + \cdots, \end{aligned} \tag{56}$$

and

$$\begin{aligned} y(\sigma_3, t) &= -1 - \frac{4}{3}t - \left(\frac{2}{9} - 2\sigma_3\right)t^2 + \left(\frac{2}{81} + \frac{2}{3}\sigma_3 - 3\sigma_3^2\right)t^3 + \left(\frac{2}{81} - \frac{1}{9}\sigma_3 - \frac{3}{2}\sigma_3^2 + \frac{9}{2}\sigma_3^3\right)t^4 + \cdots, \\ z(\sigma_3, t) &= 1 + \frac{2}{3}t - \sigma_3 t^2 - \left(\frac{10}{81} - \frac{3}{2}\sigma_3^2\right)t^3 + \left(\frac{5}{729} + \frac{5}{9}\sigma_3 - \frac{9}{4}\sigma_3^3\right)t^4 + \cdots. \end{aligned} \tag{57}$$

A straightforward calculation shows that these two expansions are nothing but the expansion of curve Γ_1 transformed by k_ϵ and k_ϵ^2. The parameters σ_i in (56) and (57) are also just reparameterization parameters, like σ in (49) and (50). The slopes at $(y, z) = (-1, 1)$, corresponding to the three curves Γ_i, are just the first-order term in (53), (56) and (57), namely $(\frac{2}{3}, \frac{2}{3})$, $(\frac{2}{3}, -\frac{4}{3})$, and $(-\frac{4}{3}, \frac{2}{3})$. They correspond exactly to the three edges of the triangle built from the three confluent fixed points of k_ϵ^3 when $\epsilon \to 3$.

Since the three Γ_i's are on the same footing, let us restrict to Γ_1. With the $\sigma = -\frac{2}{9}$ choice, the expansion corresponding to Γ_1 (see (53) and (54)), actually verifies, as a consequence of (55), the exact nonlinear functional equation:

$$\left(y\left(\frac{t}{1+t}\right) + y(-t) + 4\right)(y(-t) + 3)y(t) + (y(-t) - 1)\left(y\left(\frac{t}{1+t}\right) - 3y(-t) - 4\right) = 0. \tag{58}$$

This equation is obtained from the equality of the y-components of k_ϵ^3 coming, respectively, from (47) and (48). Of course one can obtain another, similar, nonlinear functional equation, deduced from the equality of the z-component of k_ϵ^3 in (47) and (48):

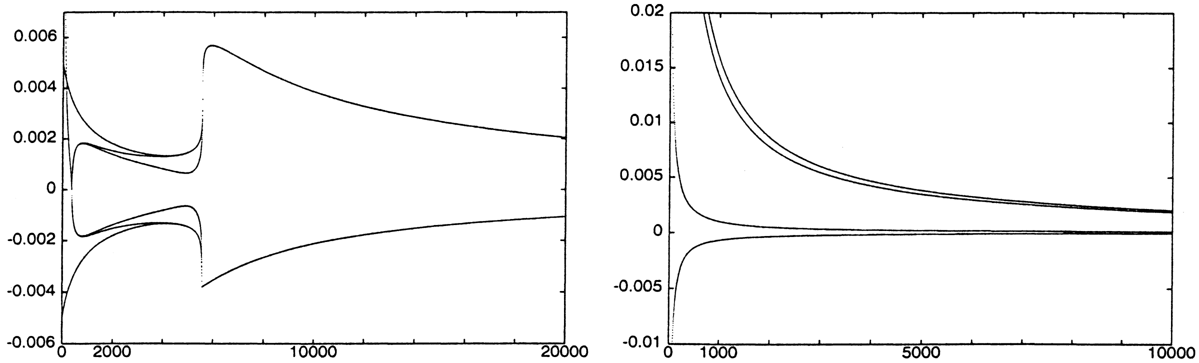

Fig. 21. Left: $L_i^{(N)}$'s, as a function of N, for orbit of Fig. 20 (right). Right: The $L_i^{(N)}$'s, as a function of N, for a generic orbit of the point $y = 0.8, z = -1.2$.

$$\left((1 - y(-t))y\left(\frac{-t}{1+t}\right) - y(t)y(-t) - 3y(t) + 2y(-t) - 2\right)$$
$$\times(y(t)y(-t)^2 + 4y(t)y(-t) - 3y(-t)^2 - 4y(-t) + 3y(t) + 7) + (4y(t)y(-t)$$
$$+12y(t) - 4 + 4y(-t))(2y(-t) - 2 - 3y(t) - y(t)y(-t)) = 0. \quad (59)$$

One easily verifies that the expansion of $y(t)$, at higher orders (see Appendix C), is actually a solution of these two functional equations (58) and (59).

6.2. *Checking numerically the divergent series*

Similarly to what has been done for the neighborhood of the point at infinity for various values of ϵ, it is worth considering a single orbit near the fixed point of mapping (1) for $\epsilon = 3$. The orbit corresponding to Fig. 20 (left) originates from the iteration of an initial point $(y, z) = (1 + \epsilon_1, -1 + \epsilon_1)$ where ϵ_1 is very small (tangent to the true curve parameterized by (53) and (54)). One finds that the points of this orbit are in perfect agreement (see Fig. 20 (left)) with the plot of the curve parameterized by (53) and (54), up to order 36. Of course, this curve is just a polynomial approximation of the transcendental curve corresponding to the divergent series (53) (see also (C.1) in Appendix C). The polynomial curve, parameterized by (53) up to order 36, makes two corners near $(y, z) \simeq (0.8, -1.2)$ and near $(y, z) \simeq (1.2, -0.8)$ when the last, t^{36}, term becomes dominant, and thus differs from the true transcendental curve associated to the divergent series (53) (see also (C.1) in Appendix C). After all, asymptotic series are not so bad: despite their monstrous character, one sees that they can be very well, and simply, approximated.

Fig. 20 (right) corresponds to another initial point of the previous form $(y, z) = (1 + \epsilon_1, -1 + \epsilon_1)$ but with ϵ_1 slightly larger (and therefore one is not exactly on the transcendental curve corresponding to the divergent series (53) anymore). One is back to a quite generic orbit of the foliation depicted in Fig. 19. One sees, however, in this region near the fixed point that such a generic curve of the foliation gets extremely close to the transcendental curve corresponding to the divergent series (53) and (54). Not surprisingly, our Lyapunov program, performed on the orbits of Fig. 20, do suggest Lyapunov characteristic exponents also equal to zero (see Fig. 21).

The orbits of k_ϵ^3, in the real (y, z)-plane, build a very regular phase portrait which looks very much like a foliation of the plane in curves [32]. The previous expansions (49) and (50) give some hint on only three of these curves. It would be interesting to perform similar calculations for the curves not including the fixed point $(-1, 1)$. This remains to be done. The parameterization of, at least, the three curves Γ_i corresponding to the divergent series, seems to exclude a parameterization in algebraic elliptic curves. Actually, using a systematic method well suited for two-dimensional rational transformations, introduced in [32], we have not been able to find any algebraic invariant corresponding to a possible linear pencil of this very regular foliation. This seems to correspond exactly to the notion of non-algebraic integrability [34] developed by Rerikh [81–83]. In fact, complexity growth calculations, performed for this $\epsilon = 3$ case, do show [35] the same value for the complexity growth λ, namely $1.61803\ldots$, than for the other generic values of ϵ. The system is actually chaotic for $\epsilon = 3$, even if its restriction to the real (y, z)-plane is extremely regular (the real topological entropy being zero [35]). The corresponding function which gives nice real curves corresponds to a divergent series which is certainly quite monstrous in the non-real (complex) plane. One can imagine that this kind of function corresponding to divergent series is actually compatible with pictures like the one of the Vague Attractor of Kolmogorov (see the VAK in [84] or the Nested KAM tori [85], p. 441) together with the occurrence of a nice curve in the real space. The occurrence of such divergent series solves the paradox of the compatibility between a regularity of the (real) phase portrait together with a chaotic (complex) dynamics (complexity growth $\lambda \simeq 1.61803$). This example shows that simple functional equations, yielding curves, or even foliation in curves, but only for real values of the variables, are actually compatible with a chaotic dynamical system. One can actually calculate, order by order, all the coefficients of the divergent series (53) from the functional equations (58), however, the growth of the computing time is exponential, not polynomial (see also Appendix C).

7. A simple birational deformation breaking the measure-preserving property and its associated Lyapunov exponents

In view of the previous results, one may think that reversibility, especially in the algebraic framework of birational transformations, leads naturally to systems of zero metric entropy. Let us see, in this section, that this is not the case, and that the previous zero (or at least very small, etc.) metric entropy is in fact a consequence of the specific character of transformation (1) and in particular its measure-preserving property.

Let us consider a simple birational transformation which is a simple birational deformation of the birational transformation (1):

$$k_{\epsilon,\beta} : (y, z) \to \left(\frac{z + 1 - \epsilon}{1 + \beta z}, y\frac{z - \epsilon}{z + 1} \right). \tag{60}$$

One easily verifies that transformation (60) is actually birational and has [35] still a growth complexity $\lambda \simeq 1.61803$, the generating function of the degrees of the numerator of the z-components being

$$G(t) = \frac{1 + t}{1 - t - t^2} = 1 + 2t + 3t^2 + 5t^3 + 8t^4 + 13t^5 + 21t^6 + 34t^7 + 55t^8 + 89t^9 \\ +144t^{10} + 233t^{11} + 377t^{12} + \cdots . \tag{61}$$

This birational deformation does not modify the growth-complexity λ of transformation (1) ($\lambda \simeq 1.61803$), but does modify the phase portrait: for instance one easily verifies that the determinant of the Jacobian matrix of $k^N_{\epsilon,\beta}$, evaluated at a fixed point of $k^N_{\epsilon,\beta}$, is no longer equal to 1. This property [36] of the determinant being equal to 1 was, in fact, a consequence of the fact that transformation (1) is a measure-preserving map.

[34] Non-algebraic integrability of the Chew–Low reversible dynamical system of the Cremona type [79,80] has been addressed by Rerikh [81–83].

[35] Generically for the generic values of ϵ and for many non-generic values of ϵ ($\frac{1}{3}, \frac{1}{4}, 1, \ldots$) except $\epsilon = -1$, for which one recovers the integrable $(1 - t)$ singularity.

[36] This measure-preserving property obviously helps the systems to have elliptic trajectories around the fixed points of k^N_ϵ and the mapping to be a diffeomorphism tangent to identity at the fixed point at infinity, these two properties being crucial to have a very regular phase portrait, yielding a very weak metric entropy.

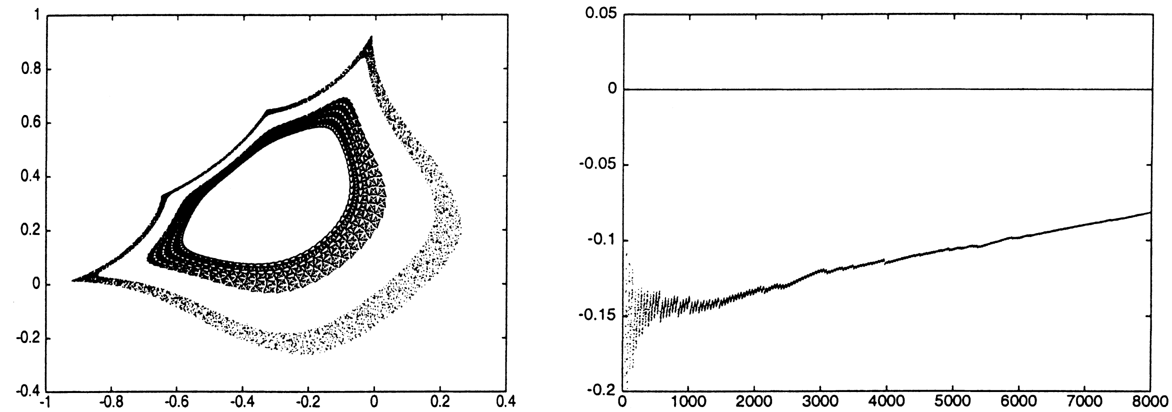

Fig. 22. Left: An expanding spiraling orbit of the initial point $y_0 = 0.1$, $z_0 = -0.5$ for $\epsilon = 0.34$ and $\beta = 1 \times 10^{-4}$. We have represented the first 10 000 iterations (inside) and the 10 000 iterations after 50 000 iterations (outside). Right: The $L_i^{(N)}$'s, as a function of N, for the previous orbit.

Let us study the birational transformation (60), comparing its phase portraits with the phase portraits of transformation (1), and also comparing the corresponding Lyapunov exponents. Let us first see the birational transformation (60) as a deformation of (1), and let us restrict ourselves to small values of the deformation parameter β. For $\beta \simeq 1 \times 10^{-4}$, the curves in the elliptic regular region (see Fig. 4) become (as a consequence of the determinant of the Jacobian matrix of $k^N_{\epsilon,\beta}$, evaluated at a fixed point of $k^N_{\epsilon,\beta}$, being no longer equal to 1) orbits spiraling around the fixed elliptic points.

Fig. 22 (left) represents such an expanding spiraling orbit (more precisely two parts of this orbit, namely the first 10 000 iterations and the 10 000 iterations after 50000 iterations). The orbit is in expansion from an orbit inside (see the first 10 000 iterations) to the shield-graft limit of this region. Fig. 22 (right) represents the $L_i^{(N)}$'s, as a function of N, for the previous orbit. The linearization, near the (expansive) fixed point at the middle of this region, gives a Jacobian matrix with two (complex conjugate) eigenvalues of modulus very close to 1, but slightly larger than 1: this is in fact in agreement with Fig. 22 (left and right).

Let us recall, for transformation (1), the partition of the (real) (y, z)-plane into the regular elliptic regions and the region associated with the point at infinity (the extension of the hyperbolic regions being very small, possibly zero).

Fig. 23 (left) represents an orbit in the region associated with the point at infinity, but in the $(Y, Z) = (1/y, 1/z)$ variables. In the (y, z) variables the orbit is more fuzzy as compared to the equivalent one for transformation (1). The orbit looks, at first sight, quite similar to Fig. 15 corresponding to the birational transformation (1). However, this similarity is probably just superficial: the point at infinity which is a fixed point of mapping (1), is not a fixed point of mapping (60) any longer. The region of the (Y, Z)-plane, associated with the point at infinity, is more subtle than the obvious, previously mentioned (see Fig. 22), expanding, or contracting, regions around fixed points. In order to understand, more clearly, what is really going on in this region associated with the point at infinity, let us perform a much larger deformation of transformation (1), considering $\beta = 1.1$.

One finds some strange attractor (see Fig. 24 (left)), the calculations of the Lyapunov characteristic exponents yielding a negative value for one of the two $L_i^{(N)}$'s, but also a small, but positive, Lyapunov exponent (see Fig. 24 (right) and the insert corresponding to a magnification of the positive $L_i^{(N)}$'s). One thus sees, with this example, that one may have a non-zero metric entropy for a birational transformation having the same topological entropy as (1). The previously noticed zero (or, at least, very weak) metric entropy is not a consequence of the birationality of the transformation only: the measure-preserving property is certainly crucial.

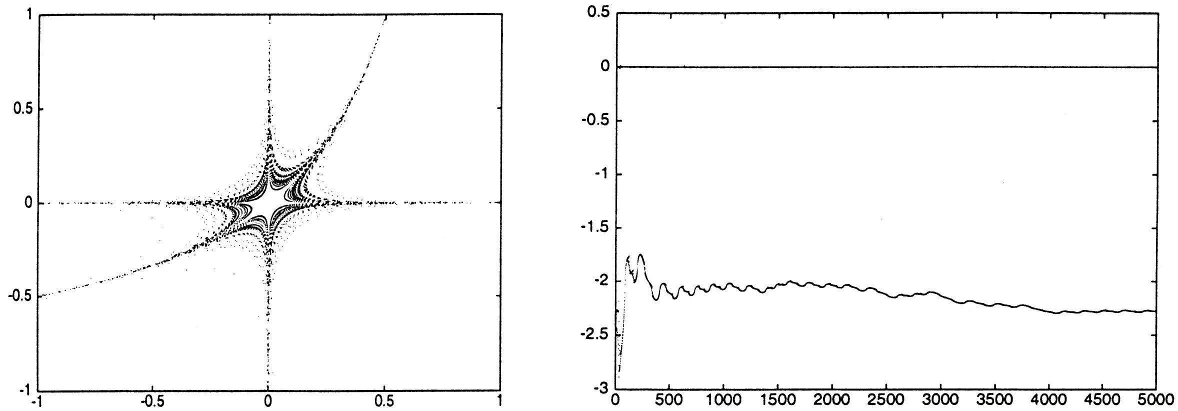

Fig. 23. Left: An orbit of the initial point $y_0 = 11$, $z_0 = -17$ for $\epsilon = 0.34$ and $\beta = 1 \times 10^{-4}$, in the Y and Z variables. Right: The $L_i^{(N)}$'s, as a function of N, for the previous orbit.

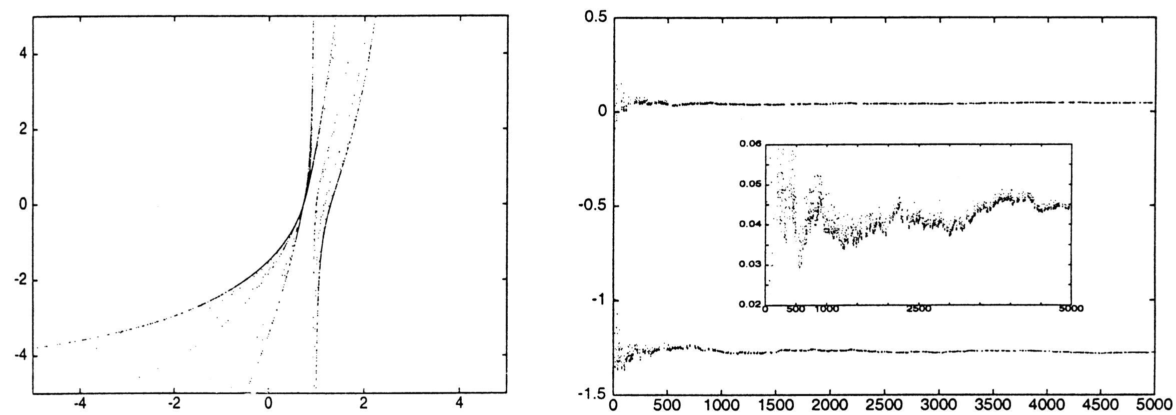

Fig. 24. Left: An orbit of the initial point $y_0 = 0.82$, $z_0 = 0.456$ for $\epsilon = 0.34$ and $\beta = 1.1$. Right: The $L_i^{(N)}$'s, as a function of N, for the previous orbit. The insert corresponds to a magnification of the positive $L_i^{(N)}$.

8. A simple rational deformation breaking the reversibility property and its associated Lyapunov exponents

The breaking of reversibility, linked to some loss of memory, is at the origin of many phenomena associated with chaos (occurrence of strange attractors, etc.). Let us consider another deformation of the birational transformation (1), namely a non-invertible rational transformation:

$$(y, z) \rightarrow \left(\frac{z + 1 - \epsilon}{1 + \beta y}, y \frac{z - \epsilon}{z + 1} \right). \tag{62}$$

One easily verifies that the rational transformation (62) has [37] a growth complexity $\lambda = 2$, the generating function of the degrees of the numerator of the z-components being

[37] Generically for the generic values of ϵ and for many non-generic values of ϵ ($\frac{1}{3}, \frac{1}{4}, 1, \ldots$), except $\epsilon = -1$, for which one recovers the $1 - t - t^2$ denominator and for which the mapping becomes birational again.

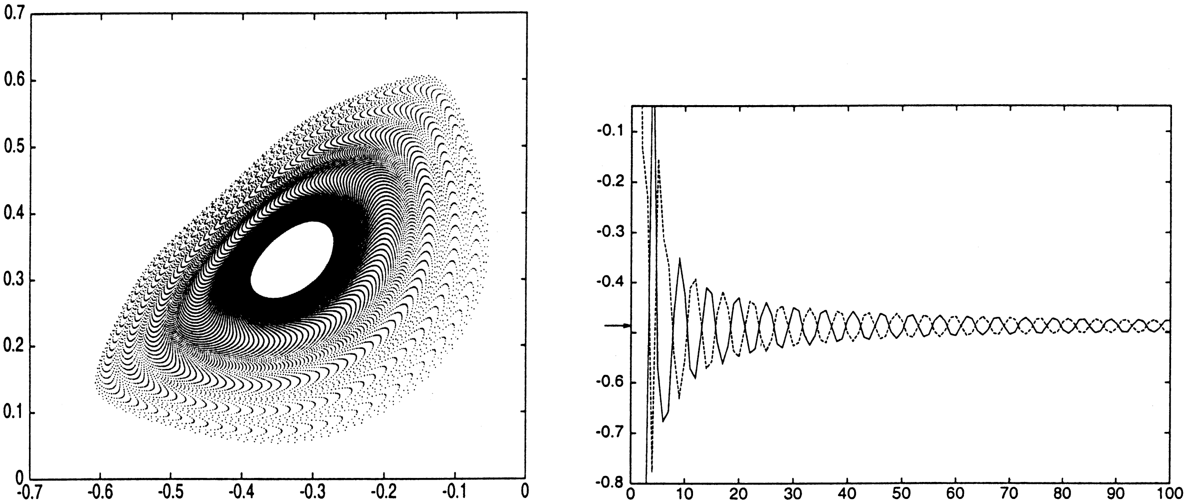

Fig. 25. Left: One confined orbit for $\beta = 1 \times 10^{-4}$ and $\epsilon = 0.34$. Right: $L_i^{(N)}$, as a function of N, for another annulus-like orbit of the initial point $y_0 = -0.3$, $z_0 = 0.4$ for $\epsilon = 0.34$ and $\beta = 1.1$. The expected negative limit for the $L_i^{(N)}$'s equals to $\simeq -0.486315$ is indicated by an arrow.

$$G(t) = \frac{1 - 2t^2 + 2t^5}{(1-t)(1+t)(1-2t)} = 1 + 2t + 3t^2 + 6t^3 + 11t^4 + 24t^5 + 47t^6 + 96t^7 + 191t^8 + 384t^9 + 767t^{10} + 1536t^{11} + \cdots . \quad (63)$$

For $\epsilon = -1$, the rational transformation (62) becomes birational [38] and the previous generating function reads (up to order 12)

$$G(t) = \frac{1 - 2t^2 + t^5 + t^6}{(1 - t - t^2)(1 - t^2)}. \quad (64)$$

The analysis of this (generically) rational (but not birational) deformation of transformation (1) gives, at first sight, results similar to the ones of Section 7. The curves of the regular elliptic region of Fig. 4, again, become spiraling orbits.

Fig. 25 (left) shows such a spiraling orbit, slowly contracting towards a central fixed point. For another orbit (not represented here, corresponding to the $L_i^{(N)}$'s of Fig. 25 (right)), one also gets such a spiraling orbit quickly contracting to a fixed point. These results are in agreement with the linearization around the fixed point. For the second orbit, one expects a negative limit for the $L_i^{(N)}$'s equal to $\simeq -0.486315$, in quite good agreement with the calculations of the $L_i^{(N)}$'s after only 100 iterations, as shown in Fig. 25 (right).

Recalling the results of Fig. 23, one can also try to analyze the region of the point at infinity for small values of the deformation parameter β. For $\beta = 1 \times 10^{-5}$, one gets, in the (Y, Z) variables, orbits similar to the orbit of Fig. 23 (left).

However, it is again clear that the similarity of Fig. 26 with Fig. 23, corresponding to $\beta = 0$, can only be superficial, since the point at infinity is not a fixed point of mapping (62) anymore. Despite these superficial similarities in the

[38] Its inverse transformation is a simple polynomial transformation, namely $(y, z) \to (z, -2 + y + \beta yz)$ and the generating function of the degrees of the numerator of the z-components becomes $G(t) = (1 + t - 2t^3 - t^4)/(1 - t - t^2)$, the $1 - t - t^2$ denominator being a direct consequence of the linear recursion on the degree: $d_{n+1} = d_{n-1} + d_n$. For $(y, z) \to (z, -2 + y + \beta y^{\mu} z^{\rho})$ one would have a $1 - \rho t - \mu t^2$ denominator.

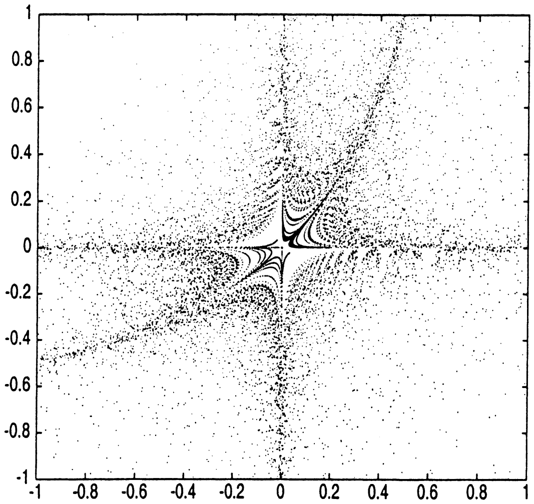

Fig. 26. One orbit for $\beta = 1 \times 10^{-5}$ for $\epsilon = 0.34$.

region associated with the point at infinity, it is however worth noticing that, trying to calculate the corresponding Lyapunov characteristic exponents $L_i^{(N)}$'s, and plotting them as a function of N, one gets quite different behaviors for the $L_i^{(N)}$'s, for the birational situation $\beta = 0$ and for $\beta = 1 \times 10^{-6}$, even if $\beta = 1 \times 10^{-6}$ yields orbits visually, almost indistinguishable from the $\beta = 0$ ones for the first 3×10^4 iterations (see Fig. 27).

The number of iterations where the systems feels the irreversibility can be estimated, for this particular orbit, to 1×10^4 iterations. These results confirm the crucial role played by the reversibility in the analysis of the Lyapunov characteristic exponents of birational transformations. Let us consider larger values of β in order to better understand the dynamics. When β is not very small, the phase portrait often becomes quickly trapped by some fixed points to which all the orbits quickly converge with spiraling orbits, however, for some values of β, one can see that there

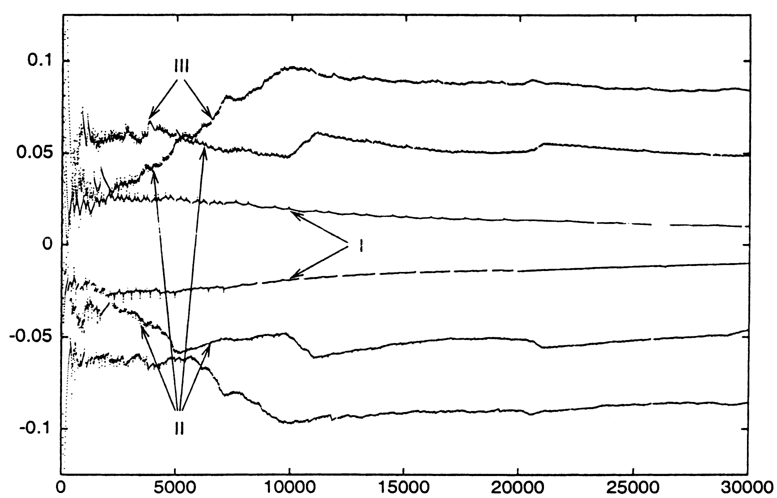

Fig. 27. The $L_i^{(N)}$'s, as a function of N, for the birational transformation (1) for $\epsilon = 0.34$ and $\beta = 0$ (indexed by (I)), and the rational transformation (62) $\beta = 1 \times 10^{-5}$ (indexed by (III)) and for $\beta = 1 \times 10^{-6}$ (indexed by (II)).

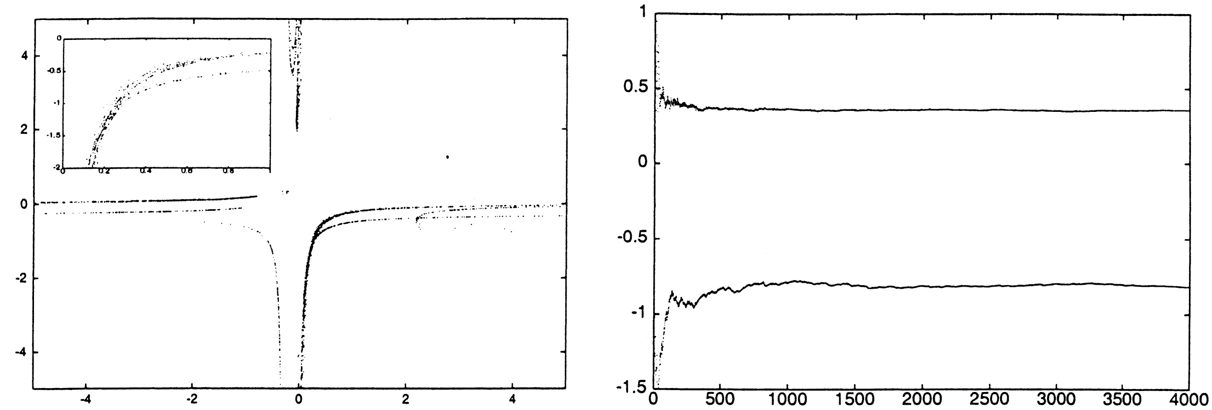

Fig. 28. Left: An orbit of the initial point $y_0 = -1.6$, $z_0 = 0.15$ for $\epsilon = 0.34$ and $\beta = 1.1$. The insert corresponds to a zoom of the strange attractor. Right: The $L_i^{(N)}$'s, as a function of N, for the previous orbit.

exists (at least) one strange attractor located in the region associated to the point at infinity, previously described for $\beta = 0$. The occurrence of this strange attractor is confirmed by the Lyapunov's calculations yielding, clearly, a positive Lyapunov characteristic exponent (see Fig. 28).

Let us consider the strange attractor which corresponds to $\epsilon = 0.333333$ and $\beta = 0.5$: this attractor is a very skinny attractor, that we will not show here. Let us recall the algebraic invariant (45) corresponding to the integrable $\epsilon = \frac{1}{3}$ case ($\beta = 0$), but written in the (y, z) variables as

$$\Delta(y, z, \tfrac{1}{3}) = \frac{(5 + 3z - 3y + 9yz)(1 - z - y + 3yz)(1 + z - y - 3yz)(1 + z + y + 3yz)}{(1 + z - y)^2} = \rho.$$

An evaluation of the $\epsilon = \frac{1}{3}$ algebraic invariant $\Delta(y, z, \frac{1}{3})$ for the successive points of this skinny strange attractor corresponding to $\epsilon = 0.333333$ and $\beta = 0.5$, shows, in Fig. 29 (left), a quite remarkable spectrum of discrete values of $\Delta(y, z, \frac{1}{3})$.

Actually, these singled-out values of $\Delta(y, z, \frac{1}{3})$ seem to correspond to finite-order orbits (for instance k^{10} = identity). Of course, it is clear that the attractor cannot be reduced to such a finite set of values. This is just a first

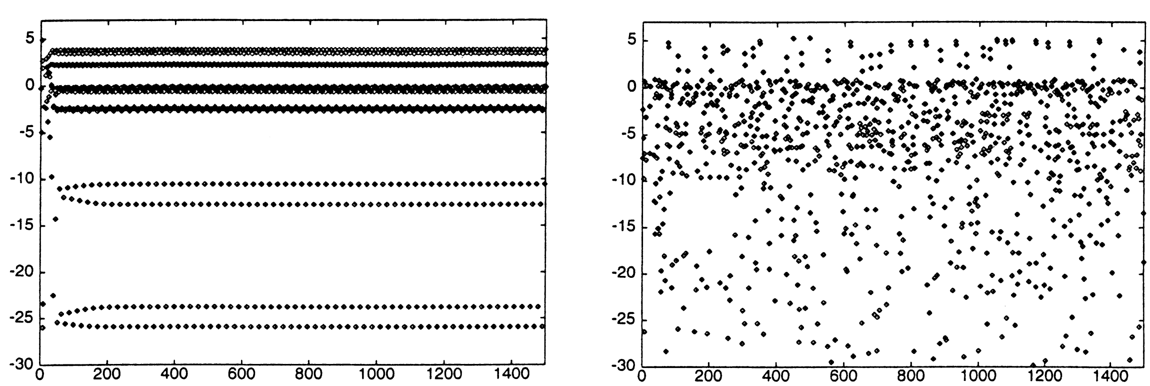

Fig. 29. Left: $\Delta(y, z, \frac{1}{3})$, as a function of the number of iterations N, corresponding to the strange attractor orbit associated with $\epsilon = 0.333333$ and $\beta = 0.5$. Right: $\Delta(y, z, \frac{1}{3})$, as a function of the number of iterations N, corresponding to the strange attractor orbit of Fig. 28.

approximation of the true orbit. However, one recovers, here, the standard interpretation of strange attractor as a limit of sets of finite-order fixed points in the infinite-order limit. On the other hand, Fig. 29 (right) gives $\Delta(y, z, \frac{1}{3})$, as a function of the number of iterations N, for the strange attractor orbit of Fig. 28. In that case, it is clear that the distribution of $\Delta(y, z, \frac{1}{3})$ is much more involved as compared with the previous distribution for the skinny attractor.

Recalling Figs. 16 and 17 or Fig. 18 (right) also giving $\Delta(y, z, \frac{1}{3})$, as a function of the number of iteration, one sees a drastic difference with the previous analysis performed for strange attractors (see Fig. 29): for strange attractors one jumps, all the time, from one value of $\Delta(y, z, \frac{1}{3})$ to another one belonging to some, more or less, complicated spectrum of values, while for the orbits described in Figs. 16 and 17 or Fig. 18 (transcendental-like curves? etc.), one seems to explore various values of $\Delta(y, z, \frac{1}{3})$ consecutively.

9. Conclusion

The results presented here seem to be in agreement with very small metric entropies for birational transformation (1) for any value of the parameter ϵ. The possibility that the metric entropy could actually be very small, for most of the invariant measures, for a large set of birational measure-preserving transformations generated by involutions is not excluded.

Calculating characteristic Lyapunov exponents amounts to performing local calculations (like derivatives: calculating a Jacobian matrix for the Nth iterate k^N, etc.) yielding floating numbers, while the topological approach amounts to calculating global quantities encoded by integers like some number of intersections, or number of fixed points, wherever these points and intersections are (very far away, or very close from each other, etc.). In the metric approach, the question of the actual localization of these points is crucial (one can imagine to neglect elliptic regions of very small extensions, etc.), this question is irrelevant in the topological approach. This gap between local and global (or real functional analysis versus complex projective, or metric versus topological) approach can be narrowed by some assumptions on the density of periodic orbits at infinity (see the work of Fornaess and Sibony [86,87] on biholomorphic transformations in C^N), or some ergodic hypothesis which are quite hard to control. With some birational transformations which naturally occur in lattice statistical mechanics [23], namely birational measure-preserving transformations generated by involutions we seem to be able to get a large set of examples of discrete dynamical systems which can be topologically chaotic when they seem to be metrically almost quasi-periodic. This measure-preserving property is a necessary (but probably not sufficient) condition to have a phase portrait so regular [39] that it yields very weak metric entropy.

We have tried, here, to understand such a metric almost periodicity together with a topological chaos situation on a very simple (but non-trivial) birational toy example where it has been seen that this situation seems to be the consequence of two phenomena. First, there is no chaotic hyperbolic regions (infinite set of homoclinic points, intersections of stable and unstable manifolds) for this two-dimensional birational example: an orbit can be locally hyperbolic but, globally, it will be elliptic. Thus, the whole two-dimensional (real) space seems to be partitioned into regular elliptic regions, where one can easily understand that the metric entropy will be zero, and a region associated with the point at infinity. Secondly, this region associated with the point at infinity, corresponds to some kind of transcendental foliation, or, at least, to a quasi-foliation in curves (see Section 5.2). Again, because of this (quasi-)foliation, the metric entropy could be zero, or in any case, should be very small. The $\epsilon = 3$ situation is an extreme example of such a situation: the topological entropy is non-zero but one seems to have a zero real topological entropy when the mapping is restricted to real variables. The $\epsilon = 3$ mapping has certainly zero metric entropy, the transcendental curves of the foliation of the two-dimensional space, satisfying remarkable nonlinear functional equations. As a consequence of

[39] This measure-preserving property has the following consequence: the Jacobian of k^N is equal to 1 at every fixed point of k^N, for any N.

this foliation, there is no serious metric chaos. However, the transcendental character of this foliation corresponds to a clear exponential computing complexity: to sum up, and in simple words, a topological chaos is perfectly compatible with a metric quasi-periodicity. Recalling Fornaess and Sibony's [86] assumption on the density of periodic orbits at infinity, the possible existence of a foliation for our birational example is actually a situation where this density is very particular.

The results presented here may look a bit paradoxical: computing Lyapunov exponents at various typical (with respect to some invariant measure ν) points one seems to always get a zero value. By the Pesin–Ruelle inequality the Lyapunov being zero means that the metric entropy $h(\nu)$ of the invariant measure ν would be zero. However, the topological entropy is the supremum of these $h(\nu)$ taken over all k_ϵ-invariant measures ν, and is clearly non-zero: therefore, there must exist some invariant measure ν and some points somewhere such that the Lyapunov exponents of the corresponding orbits are non-zero. We have no idea where such points could be. In particular, we have no idea where points such that the Lyapunov exponents of their orbits could be of the order of the real topological entropy $\simeq \log(h_{\mathrm{real}})$ or of the order of the topological entropy $\simeq \log(h)$.

Of course, all the results presented here are very preliminary. One can, however, hope that birational measure-preserving transformations generated by involutions could thus allow to better understand the gap between the topological universe and the measure universe, i.e. between the topological description and the probabilistic description of discrete dynamical systems. Corresponding to topological chaos and weak metric chaos, some birational measure-preserving transformations generated by involutions, might be seen as a possible frontier between these two universes. Despite their reversible and algebraic character, birational measure-preserving transformations generated by involutions correspond to a huge set of transformations. It would be interesting to see if the "topological-chaos with metric-weak-chaos" situation, described here, is, beyond the measure-preserving property, also a consequence of the specificity of the mapping considered here, in particular its two-dimensional character and, especially, the structural instability of the point at infinity.

Acknowledgements

One of us (JMM) would like to thank P. Lochak and J.-P. Marco for illuminating discussions on symbolic dynamics and on non-hyperbolic discrete dynamical systems and R. Quispel for precious discussions on mappings generated by reflections and, especially, measure-preserving mappings. We thank the referees for a very careful reading of our manuscript and S. Hassani for many useful comments.

Appendix A. Less universal Arnold complexities

Let us calculate a modified Arnold complexity, $\tilde{A}_N$, corresponding to a calculation with a finite, not too large, precision (say 1000 digits, etc.) and to intersection counting in some finite box. Of course, one also calculates $\tilde{A}_N^{1/N}$ which is supposed to have a large N limit. This introduces a less universal (more metric), scale-dependent, notion of (real Arnold) complexity. Of course, this can also be introduced for the counting of the real fixed points of k_ϵ^N, i.e. for the calculation of the real topological entropy, thus yielding a far less universal new real topological entropy, closer to a notion of visual complexity as it can be seen on the phase portraits (see Fig. 4). Such new complexity notions will take into account a more metric point of view, which amounts to saying that an elliptic region of a too small extension could be neglected, the extension of this region being a weighting parameter. This is a way to introduce a notion of measure of these topological structures. Let us compare such calculations performed with only 1000 digits, with the infinite precision calculations of Fig. 1. For instance, let us consider $\tilde{A}_{13}^{1/13}$, corresponding to

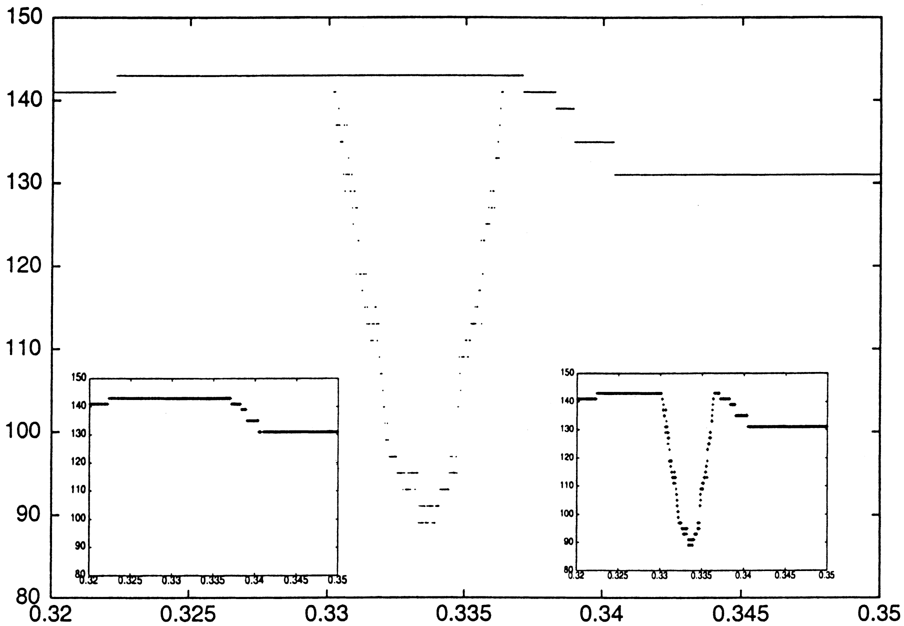

Fig. 30. $\tilde{A}_{13}^{1/13}$, as a function of ϵ, corresponding to the counting of Arnold intersections with a precision of 1000 digits together with $\mathcal{A}_{13}^{1/13}$ corresponding to an infinite precision calculation, in the interval $[0.32, 0.35]$. The right insert corresponds to the 1000 digits calculation of $\tilde{A}_{13}^{1/13}$ and the left insert corresponds to the infinite precision (exact) calculation of $\mathcal{A}_{13}^{1/13}$.

the counting of Arnold intersections with a precision of 1000 digits, which, from time to time, cannot discriminate between some points that are too close and count them as a single point. The plot of $\tilde{A}_{13}^{1/13}$, as a function of ϵ, gives a result almost indistinguishable from Fig. 1, except in the neighborhood of the non-generic $\epsilon = 1/m$ values (as well as the $\epsilon = (m-1)/(m+3)$). Let us give here a plot corresponding to such a calculation of $\tilde{A}_{13}^{1/13}$, as a function of ϵ, performed with only 1000 digits around $\epsilon = \frac{1}{3}$.

One remarks that the neighborhood of the $\epsilon = \frac{1}{3}$ value is singled out in such a calculation, but in a quite different way as compared to the way the $\epsilon = 1/m$ values are singled out in Fig. 1: near this $\epsilon = \frac{1}{3}$ value, the visual complexity $\tilde{A}_{13}^{1/13}$ becomes smaller. One has a similar phenomenon around all the $\epsilon = 1/m$ values, yielding a decrease of $\tilde{A}_{13}^{1/13}$ similar to the one in Fig. 30, around all these values. Around these $\epsilon = 1/m$ values, one also remarks another phenomenon which has some impact on the visual complexity, as it can be seen on the phase portrait of Fig. 4 for instance. One actually finds out that several of these Arnold intersections migrate to infinity (when N gets large) thus being out of the frame of a given phase portrait (like Fig. 4 for instance). For $\epsilon = \frac{1}{4}$, around two-third of the Arnold intersections of the line $y = \frac{1}{2}(1-\epsilon)$ with its 13th iterate correspond to z values in the interval $[-1, +1]$, most being close to $z \simeq -0.66$ or $z \simeq -0.62$, however, some z values obviously do not belong to this narrow box ($z \simeq -150.37, z \simeq +71.87, \dots$). We do not want to analyze, here, in detail this distribution of z values when $N \to \infty$ together with $\epsilon \to 1/m$. It is clear that one can introduce many complexities $\mathcal{A}_{R,N}^{1/N}$, corresponding to the counting of Arnold intersections inside a given interval $[-R, +R]$, or inside a given disk of radius R. Of course, there are many (not very well-defined, etc.) ways to change the real topological entropy, or the real Arnold complexity, into a less universal quantity turning it into a more metric quantity, which tries to fill the gap between the metric (measure) point of view and the topological point of view.

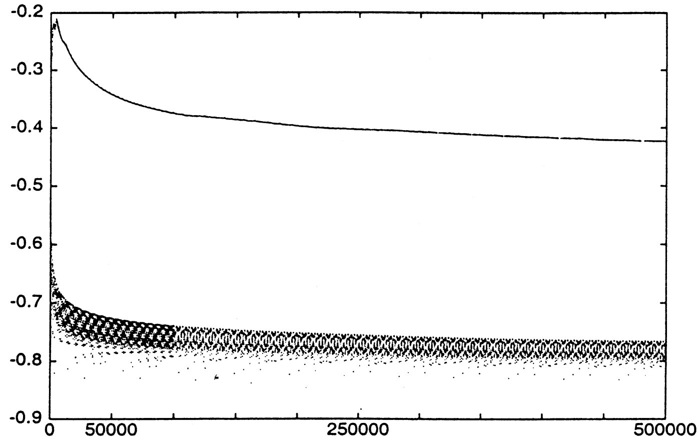

Fig. 31. $\alpha_N^{(i)}$'s, as functions of the number of iterations N, for $\epsilon = 0.49$, for two orbits close to the diamond-shaped frontier of Fig. 9.

Appendix B. Zero limit of the Lyapunov exponents

In Section 4.5 (corresponding to hyperbolic points near the spray-like region) the $L_i^{(N)}$'s seem, phenomenologically, to behave like

$$L_i^{(N)} = \frac{\ln(|\lambda_i^{(N)}|)}{N} \simeq N^{\alpha}, \quad i = 1, 2, \tag{B.1}$$

where the exponent α seems to be the same for $L_1^{(N)}$ and $L_2^{(N)}$. In this respect, let us introduce the two variables $\alpha_N^{(i)}$ defined by

$$\alpha_N^{(i)} = \frac{\ln(|L_i^{(N)}|)}{\ln(N)}, \qquad i = 1, 2, \tag{B.2}$$

which have the limit $\alpha_N^{(i)} \to \alpha$, if the phenomenological relation (40) is actually valid. Non-zero Lyapunov exponents correspond to $\alpha = 0$ for which one has a non-zero finite limit for the $L_i^{(N)}$'s. The $\alpha = -1$ value corresponds, for instance, to the $\ln(|\lambda_i^{(N)}|)$'s being bounded by a value independent of N (this is the case for elliptic orbits). Let us plot the $\alpha_N^{(i)}$'s, as a function of the number of iterations N, for the orbit in the spray-like region, but near the diamond shaped frontier (indexed by (II) in Fig. 10).

Fig. 31 is, up to 5×10^5 iterations, in quite good agreement with the phenomenological relation (40). Of course, one could argue that the $\alpha_N^{(i)}$'s seem, again, to behave like another power law $\simeq A + BN^{-\alpha'}$, thus introducing further corrections. Our point here is just that the extensivity of the $\ln(|\lambda_i^{(N)}|)$'s is certainly not satisfied: we have here an under-extensive behavior for the $\ln(|\lambda_i^{(N)}|)$'s yielding Lyapunov exponents equal to zero. Fig. 31 gives the $\alpha_N^{(i)}$'s, as functions of the number of iterations N, for two orbits close to the diamond-shaped frontier in Fig. 9. One orbit is outside the diamond-shaped frontier in the spray-like region and corresponds to the upper curve in Fig. 31, while the lower fuzzy set of data in Fig. 31 corresponds to an orbit inside the diamond-shaped frontier (see Fig. 9). Keeping in mind that the orbit inside the diamond-shaped frontier is in the elliptic region, and, especially, keeping in mind the $\theta \to \theta + \lambda$ shift interpretation of the movement on this very orbit, one can certainly argue that, in the N large limit, $\alpha_N^{(i)}$ should tend to a $\alpha_\infty = -1$ limit (bounded periodic function). This large N limit, $\alpha_\infty = -1$, is not incompatible with Fig. 31.

Appendix C. The expansion of $y(t)$ for the $\epsilon = 3$ case

Let us give here, up to order 28, the expansion of the divergent series (56) satisfying the two functional equations (58) and (59):

$$
\begin{aligned}
y(t) = &-1 + \frac{2}{3}t + \frac{2}{9}t^2 - \frac{4}{81}t^3 - \frac{67}{729}t^4 + \frac{119}{6561}t^5 + \frac{7031}{78732}t^6 - \frac{9004}{531441}t^7 - \frac{498563}{3188646}t^8 \\
&+ \frac{4012423}{133923132}t^9 + \frac{9273016087}{21695547384}t^{10} - \frac{65639286071}{781039705824}t^{11} - \frac{3919438859951}{2343119117472}t^{12} \\
&+ \frac{58702493381929}{173976594472296}t^{13} + \frac{36954492298242887}{4175438267335104}t^{14} - \frac{296783900798299309}{162842092426069056}t^{15} \\
&- \frac{1068916236137657496299}{17586945982015458048}t^{16} + \frac{3521411684134210965649}{276994399216743464256}t^{17} + \frac{873169015196420150636423}{1661966395300460785536}t^{18} \\
&- \frac{63608026457130368941111487}{572131931582183625420768}t^{19} - \frac{153262556077398234892492926167}{27462332715944814020196864}t^{20} \\
&+ \frac{2486381755277467654080184241081}{2087137286411805865534961664}t^{21} + \frac{132736579097260552611348063340597}{1857781540652266759432218624}t^{22} \\
&- \frac{4809337322739099418205059004605277}{313254752134101333288967922688}t^{23} - \frac{34666340109953257893099809606832084623}{31951984717678335995474728114176}t^{24} \\
&+ \frac{51145774987456210637000437263820857362299}{218264007606460713185087867747936256} t^{25} \\
&+ \frac{50495777020773376116907497144298407135656551}{2619168091277528558221054412975235072} t^{26} \\
&- \frac{32851079380319620883471714906166192560054779}{7857504273832585674663163238925705216} t^{27} \\
&- \frac{189183099578052801080437416188689042799128604741}{477343384635329579735787166764736591872} t^{28} + \cdots .
\end{aligned}
\tag{C.1}
$$

One easily verifies that this expansion satisfies, order by order, the functional equations (58) and (59).

Let us denote by a_n the order n coefficient of $y(t)$. From the nonlinear functional equations (58) (or (59)), one can deduce the following recursion (with $a_0 = -1$ and $a_1 = \frac{2}{3}$):

$$
\begin{aligned}
-4(i-1-2(-1)^i)a_{i-1} = &\sum_{j=1}^{i-2}(-1)^{j-i}a_j\left(-4\binom{i-1}{j-1} - 2\binom{i-2}{j-1}a_1\right) \\
&+\sum_{k=2}^{i-2}(-1)^i a_k\left(4((-1)^k-1)a_{i-k} + 2\sum_{j=1}^{i-k}(-1)^{j-k}\binom{i-k-1}{j-1}a_j\right) \\
&+\sum_{k=1}^{i-1}\left((-1)^k a_k + \sum_{p=1}^{k}(-1)^{p-k}\binom{k-1}{p-1}a_p\right)\sum_{j=1}^{i-k-1}(-1)^j a_j a_{i-k-j},
\end{aligned}
\tag{C.2}
$$

where $\binom{i}{j}$ is the binomial symbol. This recursion gives a_{i-1} in terms of the a_j's of lower order. We have calculated these coefficients up to order 300. One can numerically see that this series seems to be Borel summable. Actually, it seems that the a_n's behave asymptotically like

$$\frac{a_n}{(n+1)!} \simeq \begin{cases} -(-1)^{n/2}\alpha_{\text{even}}^n & \text{for } n \text{ even}, \\ -(-1)^{(n+1)/2}\alpha_{\text{odd}}^n & \text{for } n \text{ odd}, \end{cases}$$

with $\alpha_{\text{even}} \simeq \alpha_{\text{odd}} \simeq 0.1591$, yielding a radius of convergence, in t, around $R \simeq 6.285$.

One remarks that the numerators of the coefficients in this expansion often factorize in quite large prime numbers (in contrast with the denominators). For instance, the numerator of the coefficient of t^{25} factorizes into the product of 73, 5327767 and 131504822681376234536009451871189. The numerator of the coefficient of t^{26} factorizes into the product of 5417, 183088852209431303 and 5091366043929018731820l. The numerator of the coefficient of t^{28} factorizes into the product of 58237, 8933 and 363652022997779867691608968908050087221. This function can thus be seen to produce large prime numbers.

References

[1] E. Ott, Chaos in Dynamical Systems, Cambridge University Press, Cambridge, 1993.
[2] K.T. Alligood, T.D. Sauer, J.A. Yorke, Chaos: An Introduction to Dynamical Systems, Springer, New York, 1997.
[3] A.N. Kolmogorov, A new metric invariant of transitive dynamical systems and automorphisms in Lebesgue spaces, Dokl. Acad. Nauk SSSR 119 (1958) 861.
[4] Y.A.G. Sinai, On the concept of entropy of dynamical system, Dokl. Acad. Nauk SSSR 124 (1959) 768.
[5] R.C. Adler, A.C. Konheim, M.H. McAndrew, Topological entropy, Trans. Am. Math. Soc. 114 (1965) 309.
[6] V. Arnold, Problems on singularities and dynamical systems, in: V. Arnold, M. Monastyrsky (Eds.), Developments in Mathematics: The Moscow School, Chapman & Hall, London, 1989, pp. 261–274 (Chapter 7).
[7] P. Grassberger, I. Procaccia, Dimensions and entropies of strange attractors from a fluctuating dynamics approach, Physica D 13 (1984) 34.
[8] J.P. Eckmann, D. Ruelle, Ergodic theory of chaos and strange attractors, Rev. Mod. Phys. 57 (1985) 617.
[9] M.J. Feigenbaum, Quantitative universality for a class of nonlinear transformations, J. Statist. Phys. 19 (1978) 25.
[10] J.M. Greene, R.S. Mc Kay, S. Vivaldi, M.J. Feigenbaum, Universal behaviour in families of area-preserving maps, Physica D 3 (1981) 468.
[11] H.G.E. Hentschel, I. Procaccia, The infinite number of generalized dimensions of fractals and strange attractors, Physica A 8 (1983) 435.
[12] P. Grassberger, I. Procaccia, Dimensions and entropies of strange attractors from fluctuating dynamics approach, Physica D 13 (1984) 34.
[13] J.L. Kaplan, J.A. Yorke, in: H.O. Peitgen, H.O. Walter (Eds.), Lecture Notes in Mathematics, Vol. 730, Springer, Berlin, 1978, p. 228.
[14] F. Ledrappier, Some relations between dimension and Lyapunov exponents, Commun. Math. Phys. 81 (1981) 229.
[15] E. Lorentz, Deterministic nonperiodic flow, J. Atmos. Sci. 20 (1963) 130.
[16] J.D. Farmer, E. Ott, J.A. Yorke, The dimension of chaotic attractors, Physica D 7 (1983) 153.
[17] R.M. May, Simple mathematical models with very complicated dynamic, Nature 261 (1976) 459.
[18] M. Hénon, A two-dimensional mapping with a strange attractor, Commun. Math. Phys. 50 (1976) 69–77.
[19] J. Milnor, Non-expansive Hénon maps, Adv. Math. 69 (1988) 109–114.
[20] D. Ruelle, F. Takens, On the nature of turbulence, Commun. Math. Phys. 20 (1971) 167–192.
[21] D. Ruelle, F. Takens, Note concerning our paper: on the nature of turbulence, Commun. Math. Phys. 23 (1971) 343–344.
[22] V. Franscechini, C. Tebaldi, Sequences of infinite bifurcations and turbulences in five-mode truncation of the Navier–Stokes equations, J. Statist. Phys. 21 (1979) 707–726.
[23] S. Boukraa, J.-M. Maillard, Factorization properties of birational mappings, Physica A 220 (1995) 403.
[24] N. Abarenkova, J.-C. Anglès d'Auriac, S. Boukraa, J.-M. Maillard, Elliptic curves from finite-order recursions or non-involutive permutations for discrete dynamical systems and lattice statistical mechanics, Eur. Phys. J. B 5 (1998) 647–661.
[25] H. Meyer, J.-C. Anglès d'Auriac, J.-M. Maillard, G. Rollet, Phase diagram of a six-state chiral Potts model, Physica A 208 (1994) 223–236.
[26] S. Boukraa, J.-M. Maillard, G. Rollet, Discrete symmetry groups of vertex models in statistical mechanics, J. Statist. Phys. 78 (1995) 1195–1251.
[27] J. Diller, Dynamics of birational maps of P^2, Indiana Univ. Math. J. 45 (3) (1996) 721–772.
[28] J. Diller, Birational maps, positive currents and dynamics, Michigan Math. J. 46 (3) (1999) 361–375.
[29] Ch. Favre, Points périodiques d'applications birationnelles de P^2, Ann. Inst. Fourier Grenoble 48 (4) (1998) 999–1023.
[30] A. Russakovskii, B. Shiffman, Value distribution for sequences of rational mappings and complex dynamics, Indiana Univ. Math. J. 46 (3) (1997) 897–932.
[31] S. Boukraa, J.-M. Maillard, G. Rollet, Almost integrable mappings, Int. J. Mod. Phys. B 8 (1994) 137–174.
[32] S. Boukraa, S. Hassani, J.-M. Maillard, New integrable cases of a Cremona transformation: a finite-order orbit analysis, Physica A 240 (1997) 586.

[33] N. Abarenkova, J.-C. Anglès d'Auriac, S. Boukraa, S. Hassani, J.-M. Maillard, Rational dynamical zeta functions for birational transformations, Physica A 264 (1999) 264–293 (chao-dyn/9807014).
[34] N. Abarenkova, J.-C. Anglès d'Auriac, S. Boukraa, S. Hassani, J.-M. Maillard, Topological entropy and complexity for discrete dynamical systems, Phys. Lett. A 262 (1999) 44–49 (chao-dyn/9806026).
[35] N. Abarenkova, J.-C. Anglès d'Auriac, S. Boukraa, S. Hassani, J.-M. Maillard, From Yang–Baxter equations to dynamical zeta functions for birational transformations, in: M.T. Batchelor, L.T. Wille (Eds.), Statistical Mechanics at the Eve of the 21st Century, in Honour of J.B. McGuire on the Occasion of his 65th Birthday, Series on Advances in Statistical Mechanics, Vol. 14, World Scientific, Singapore, 1999, p. 436–490.
[36] N. Abarenkova, J-C. Anglès d'Auriac, S. Boukraa, J.-M. Maillard, Growth complexity spectrum of some discrete dynamical systems, Physica D 130 (1999) 27–42 (chao-dyn/9807031).
[37] N. Abarenkova, J.-C. Anglès d'Auriac, S. Boukraa, S. Hassani, J.-M. Maillard, Real Arnold complexity versus real topological entropy for birational transformations, J. Phys. A., in press (chao-dyn/9906010).
[38] A.N. Kolmogorov, A new invariant of transitive dynamical systems, Dokl. Akad. Nauk. SSSR 119 (1958) 861.
[39] A.G. Sinai, On the concept of entropy of a dynamical system, Dokl. Akad. Nauk. SSSR 124 (1959) 768.
[40] J.A.G. Roberts, G.R.W. Quispel, Chaos and time-reversal symmetry: order and chaos in reversible dynamical systems, Phys. Rep. 216 (1992) 63–177.
[41] H. Poincaré, Sur un théorème de géométrie, Rend. Circ. Mat. Palermo 33 (1912) 375–407.
[42] Y. Nishimura, Iteration of some birational polynomial quadratic maps of P^2. Problems concerning complex dynamical systems, Surikaisekikenkyusho Kokyuroku 959 (1996) 152–167.
[43] R. Bowen, Periodic orbits for hyperbolic flows, Am. J. Math. 94 (1972) 1–30.
[44] M. Artin, B. Mazur, On periodic points, Ann. Math. 81 (1965) 82.
[45] V. Baladi, Periodic orbits and dynamical spectra, Ergod. Theory Dyn. Syst. 18 (1998) 255–292.
[46] D. Ruelle, Thermodynamic Formalism, Addison-Wesley, Reading, MA, 1978.
[47] R. Bowen, Symbolic dynamics for hyperbolic flows, Am. J. Math. 95 (1973) 429.
[48] R. Bowen, Equilibrium States and the Ergodic Theory of Anosov Diffeomorphisms, Springer, Berlin, 1975.
[49] R. Bowen, Markov partitions for axiom: a diffeomorphisms, Am. J. Math. 92 (1970) 725–747.
[50] S. Friedland, Entropy of polynomial and rational maps, Ann. Math. 133 (1991) 359–368.
[51] C. Smale, Differentiable dynamical systems, Bull. Am. Math. Soc. 73 (1967) 747 .
[52] F. Przytycki, An upper estimation for topological entropy of diffeomorphisms, Invent. math. 59 (1980) 205–213.
[53] A. Katok, B. Hasselblatt, Introduction to the modern theory of dynamical systems, Encyclopedia of Mathematics and its Applications, Vol. 54, Cambridge University Press, Cambridge, 1995, pp. 316, 317 (Chapter 8.3) and references therein.
[54] H. Kantz, T. Scheiber, Nonlinear time series analysis, in: Cambridge Nonlinear Science Series, Vol. 7, pp. 193, 194.
[55] S.E. Newhouse, Entropy and volume, Ergod. Theory Dyn. Syst. 8 (1998) 283–299.
[56] M. Schub, Dynamical systems filtrations and entropy, Bull. AMS 80 (1974) 27–41.
[57] Y. Yomdin, Volume growth and entropy, Israel J. Math. 57 (1997) 285–300.
[58] Y. Yomdin, C^k-resolution of semialgebraic mappings. Addendum to volume growth and entropy, Israel J. Math. 57 (1997) 301–317.
[59] D. Fried, Entropy and twisted cohomology, Topology 25 (1986) 455–470.
[60] M. Marden, Geometry of Polynomials, Am. Math. Soc. Math. Surv., 2nd Edition, AMS, Providence, RI, 1966.
[61] S. Boukraa, S. Hassani, J.-M. Maillard, Properties of fixed points of a two-dimensional birational transformation, Alg. Rev. Nucl. Sci. 3 (1999) 1–16.
[62] J.-C. Yoccoz, Idées géométriques en systèmes dynamiques, in: A. Dahan Dalmedico, J.-L. Chabert, K. Chemla (Eds.), Chaos et Déterminisme, Editions du Seuil, Paris, pp. 19–42.
[63] D.T. Kaplan, J. Yorke, Chaotic behavior of multidimensional difference equations, in: Functional Differential Equations and Approximation of Fixed Points, Springer, Heidelberg, 1987.
[64] A. Renyi, Probabilistic Theory, North-Holland, Amsterdam, 1971.
[65] A.M. Lyapunov, Problème Général de la Stabilité du Mouvement, Ann. Math. Studies, Princeton University Press, Princeton, NJ, 1947.
[66] H. Kantz, T. Schreiber, Instability: Lyapunov exponents, in: Nonlinear Time Series Analysis, Cambridge Nonlinear Science Series, Vol. 7, Cambridge University Press, Cambridge, 1997 (Chapter 5).
[67] E. Bedford, M. Lyubich, J. Smillie, Polynomials diffeomorphisms of C^2. IV. The measure of maximal entropy and laminar currents, Invent. Math. 112 (1993) 77–125.
[68] Y.B. Pesin, Characteristic Lyapunov exponents and smooth ergodic theory, Russ. Math. Surv. 32 (1977) 55.
[69] M. Pollicott, Lectures on Ergodic Theory and Pesin Theory on Compact Manifolds, Cambridge University Press, Cambridge, 1993.
[70] L.-S. Young, Dimension, entropy and Lyapunov exponents, Ergod. Theory Dyn. Syst. 2 (1982) 109–124.
[71] V.I. Oseledec, A multiplicative ergodic theorem. Lyapunov characteristic numbers for dynamical systems, Trans. Moscow Math. Soc. 19 (1968) 197–231.
[72] H. Poincaré, Oeuvres, Tome II, Gauthier-Villars, Paris, pp. 772–773.
[73] S.V. Bolotin, Homoclinic orbits to invariant tori of Hamiltonian, Trans. Am. Math. Soc. Ser. 2 168 (1995) 21–90.
[74] E. Bedford, J. Smillie, Polynomials diffeomorphisms of C^2. V. Critical points and Lyapunov exponents, J. Geom. Anal. 8 (3) (1998) 349–383.

[75] A.A. Andronov, L.S. Pontryaguin, Systèmes grossiers, Dokl. Akad. Nauk. SSSR 14 (1937) 247–250.
[76] D.V. Anosov, Structurally stable systems, Proc. Steklov Inst. Math. 169 (1985) 61–95.
[77] M. Hakim, Analytic transformations of $(C^p, 0)$ tangent to the identity, Duke Math. J. 92 (1998) 403–428.
[78] B. Shawyer, B. Watson, Borel's Methods of Summability (Theory and Applications), Clarendon Press, Oxford, 1994.
[79] L. Cremona, Elements of Projective Geometry, 3rd Edition, Dover, New York, 1960.
[80] A.P. Veselov, Cremona group and dynamical systems, Mat. Zametki. 45 (1989) 118.
[81] K.V. Rerikh, Non-algebraic integrability of the Chew–Low reversible dynamical system of the Cremona type and the relation with the 7th Hilbert problem (non-resonant case), Physica D 82 (1995) 60–78.
[82] K.V. Rerikh, Algebraic geometry approach to integrability of birational plane mappings. Integrable birational quadratic reversible mappings. I, J. Geom. Phys. 24 (1998) 265–290.
[83] K.V. Rerikh, Integrability of functional equations defined by birational mappings. II, Math. Phys. Anal. Geom., submitted for publication.
[84] R.H.G. Helleman, Self-generated chaotic behavior in nonlinear mechanics, in: E.G.D. Cohen (Ed.), Fundamental Problems in Statistical Mechanics, Vol. 5, North-Holland, Amsterdam, 1980, pp. 165–233.
[85] P. Cvitanovic, Universality in Chaos, Adam Hilger, Bristol, 1989.
[86] J.E. Fornaess, N. Sibony, Holomorphic symplectomorphism in C_{2p}, Duke Math. J. 82 (1996) 309.
[87] J.E. Fornaess, N. Sibony, Complex dynamics in higher dimensions, in: P.M. Gauthier (Ed.), Complex Potential Theory, NATO ASI Series, Vol. 439, Kluwer, Dordrecht, 1994, pp. 131–186.